



HAL
open science

Detection of irrigation dates and amounts on maize plots from the integration of Sentinel-2 derived Leaf Area Index values in the Optirrig crop model

Mohamad Hamze, Bruno Cheviron, Nicolas Baghdadi, Madiop Lo, Dominique Courault, Mehrez Zribi

► To cite this version:

Mohamad Hamze, Bruno Cheviron, Nicolas Baghdadi, Madiop Lo, Dominique Courault, et al.. Detection of irrigation dates and amounts on maize plots from the integration of Sentinel-2 derived Leaf Area Index values in the Optirrig crop model. *Agricultural Water Management*, 2023, 283, pp.108315. 10.1016/j.agwat.2023.108315 . hal-04070373

HAL Id: hal-04070373

<https://hal.inrae.fr/hal-04070373>

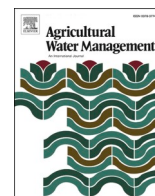
Submitted on 15 Apr 2023

HAL is a multi-disciplinary open access archive for the deposit and dissemination of scientific research documents, whether they are published or not. The documents may come from teaching and research institutions in France or abroad, or from public or private research centers.

L'archive ouverte pluridisciplinaire **HAL**, est destinée au dépôt et à la diffusion de documents scientifiques de niveau recherche, publiés ou non, émanant des établissements d'enseignement et de recherche français ou étrangers, des laboratoires publics ou privés.



Distributed under a Creative Commons Attribution 4.0 International License



Detection of irrigation dates and amounts on maize plots from the integration of Sentinel-2 derived Leaf Area Index values in the Optirrig crop model

Mohamad Hamze^{a,b,*}, Bruno Cheviron^b, Nicolas Baghdadi^a, Madiop Lo^b, Dominique Courault^c, Mehrez Zribi^d

^a French National Institute for Agriculture, Food, and Environment (INRAE), UMR TETIS, University of Montpellier, 500 Rue François Breton, CEDEX 5, 34093, AgroParisTech, Montpellier, France

^b UMR G-EAU, INRAE, 34090 Montpellier, France

^c UMR 1114 EMMAH, INRAE-Avignon université, Domaine StPaul, Agroparc, 84914 Avignon, France

^d CESBIO, University of Toulouse, CNES/CNRS/INRAE/IRD/UPS, 31400 Toulouse, France

ARTICLE INFO

Handling Editor - Dr. B.E. Clothier

Keywords:

Optirrig
Crop growth model
Irrigation
Maize
Sentinel-2
Leaf Area Index

ABSTRACT

The increase in food production due to the expansion of agricultural lands has led to the intensive use of (mainly) fresh water for irrigation. A key challenge for irrigated agriculture has thus become to optimize the use of available water resources to fit environmental constraints while satisfying the increasing food demand, achieving efficient uses of irrigation water, i.e. well-thought sequences of irrigation dates and amounts. In coherence, we developed a methodology based on the automated acquisition of Leaf Area Index (LAI) values, derived from remote sensing data, confronted with predictions drawn from the Optirrig crop growth and irrigation model, to solve the inverse problem of detecting irrigation dates and amounts, at the plot scale and for maize crops grown in the Occitanie region, France. The method consisted of seeking possible irrigation events (dates, amounts) between two cloud-free Sentinel-2 (S2) optical images and detecting the most probable of these events, responsible for the least difference between the predicted and observed, S2-derived LAI values (LAI_{S2}). The approach was first tested with synthetic noisy values to encompass the effects of errors on the observed and modeled LAI values, and these of increased duration between available observations (cases $\Delta S2 = 5, 10,$ and 15 days), promoting the possibility to use daily-interpolated LAI values as a starting point for the inverse problem ($\Delta S2$ is fixed to 10 and 15 days then values are interpolated and recorded on a 5 days basis, cases $\Delta S2 = 5 \text{ mod } 10$ and $5 \text{ mod } 15$ days, respectively). From the synthetic dataset, irrigation dates detection results showed that the best performance is obtained for $\Delta S2 = 5$ days or when using daily interpolated LAI values when $\Delta S2 = 5 \text{ mod } 10$ or $5 \text{ mod } 15$ days with an F -score near 85%. Most irrigation dates were detected with errors between 0 and 3 days, while irrigation amounts (20, 30 or 40 mm) were correctly identified in over 80% of cases, when simulating dry climatic conditions typical of the Mediterranean ring. For the documented real cases, the irrigation dates were detected with an overall recall value of 81.6% when evaluated using daily-interpolated LAI_{S2} . The irrigation amounts are correctly identified for only 28.5% of the detected irrigation dates for the plots located in Montpellier. In contrast, the detection of the irrigation amounts was not possible over the plots in Tarbes. This weakness in the detection of irrigation amounts seems related to the fact that Optirrig simulates the exact crop irrigation requirements, based on a soil water balance equation and accurate soil moisture calibration, while farmers' decisions are taken on different grounds in the field. Overall, the obtained results prove the relevance of the combined use of Optirrig and optical remote sensing data for the detection of irrigation dates, and possibly amounts, at field scale.

* Corresponding author at: French National Institute for Agriculture, Food, and Environment (INRAE), UMR TETIS, University of Montpellier, 500 Rue François Breton, CEDEX 5, 34093, AgroParisTech, Montpellier, France.

E-mail addresses: mohamad.hamze@inrae.fr (M. Hamze), bruno.cheviron@inrae.fr (B. Cheviron), nicolas.baghdadi@teledetection.fr (N. Baghdadi), madiop.lo@inrae.fr (M. Lo), dominique.courault@inrae.fr (D. Courault), mehrez.zribi@ird.fr (M. Zribi).

<https://doi.org/10.1016/j.agwat.2023.108315>

Received 7 February 2023; Received in revised form 4 April 2023; Accepted 10 April 2023

0378-3774/© 2023 The Author(s). Published by Elsevier B.V. This is an open access article under the CC BY license (<http://creativecommons.org/licenses/by/4.0/>).

1. Introduction

The world's population is expected to grow to almost 10 billion in 2050, boosting the demand for food and putting pressure on the global food supply (Godfray et al., 2010; Tilman and Clark, 2015). A huge increase in food production has been achieved through the expansion of agricultural lands and the more intensive use of inputs as natural resources (Nathan and Scobell, 2012). In this context of combined climate change and growing population, intensified agricultural systems overuse chemicals, water, plant nutrients and pesticides to increase agricultural production (DeLancey et al., 2019; Ercin et al., 2019).

In fact, irrigated agriculture is by far the main consumer of fresh water and accounts for 70% of the total freshwater withdrawals (Pokhrel et al., 2016). Water needs devoted to irrigated agriculture are even expected to increase, posing serious constraints on irrigation and freshwater availability, especially in the most water-scarce regions, such as the Mediterranean ring (Mekonnen and Hoekstra, 2014). Due to the increase of drought-affected areas, irrigation is nonetheless becoming essential for optimal crop development and production (Elliott et al., 2014; Monaco et al., 2014) while agriculture is also facing the challenge of enhancing water use efficiency by adopting new approaches of water resources management (Biagini et al., 2014; Hubert et al., 2010; Liebisch et al., 2015; Sellami et al., 2022). Research on irrigation has therefore focused on crop yield responses to water supply, seeking improved ratios between crop yield and cumulative, seasonal irrigation amounts (Chen et al., 2010; Köksal, 2011). However, identical water quotas used with different scheduling strategies, drawn from different decision rules, most likely lead to different crop yields: the fine dynamics of irrigation (dates, amounts, triggers, start and ending dates of the growing season) should be considered as of great importance in several fields related to both food security (Burney et al., 2010; Ozdogan, 2011) and water resources management (Dai and Li, 2013; Ge et al., 2013; Ouadi et al., 2021; Wu et al., 2015).

Maize (*Zea mays* L.) is one of the most important agricultural grains and a staple food in many countries (Fischer et al., 2014) which accounted for 10% of global crop production in the 1996–2010 period (Mekonnen and Hoekstra, 2016). Although potentially very productive, maize has high water and nitrogen demands, water and nitrogen stress being in turn the main constraints limiting production and productivity (Piscitelli et al., 2022; Schlüter et al., 2012). These limitations are likely to increase in the future because climatic change is expected to decrease the overall precipitation during the cropping season (Lobell et al., 2011). Increasing maize productivity in these present or future semi-arid environments will depend on the efficiency of water but also on crop management, for example through earlier sowing dates or the choice of different varieties, suggesting ad hoc, adapted irrigation strategies (García y García et al., 2009; Skuras and Psaltopoulos, 2012) and site management practices (Araus et al., 2018; Tilman et al., 2011). Finally, the stakeholders and policymakers should use all available tools in order to maximize irrigation efficiency or to supervise irrigation decisions. A possible approach for that is to combine crop growth modeling with remote sensing products (Hsiao et al., 2009; Mullen et al., 2009).

Remote sensing has been recognized as an effective tool to retrieve spatially-distributed plot-scale and regional-scale information about crop development and water requirements, leaning on the increasing availability of satellite observations with high spatial and temporal resolutions (Abuzar et al., 2015; Brown and Pervez, 2014). Biophysical variables, such as LAI, can be derived from optical data and allows to monitor the canopies' development. In fact, the methods to estimate these variables, using remote sensing data, on field crops are now well-validated (Weiss et al., 2004). In particular, satellite remote sensing has proven highly effective for mapping and monitoring irrigated areas (Demarez et al., 2019; Salmon et al., 2015; Thenkabail et al., 2005), either with optical (Gumma et al., 2011; Xiang et al., 2019) or radar sensors (Bazzi et al., 2020b; Bousbih et al., 2018; Dari et al., 2020; Gao et al., 2018; El Hajj et al., 2017; Zribi and Dechambre, 2003). Since the

synthetic aperture radar (SAR) signal is sensitive to the soil water content (Aubert et al., 2011; El Hajj et al., 2016; Hamze et al., 2021), SAR data have proven relevant for mapping irrigated areas (Bazzi et al., 2020a; le Page et al., 2020; Pervez and Brown, 2010). The fact that irrigation increases the soil water content makes the detection of irrigated areas possible using SAR data that are significantly affected by surface soil moisture (Bazzi et al., 2019; Pageot et al., 2020). In addition, several studies have shown the potential of SAR observations, mainly surface soil moisture estimates, for irrigation event detection (Aubert et al., 2013; Ouadi et al., 2021). In a recent study, Bazzi et al. (2020b) utilized Sentinel-1 SAR backscattering coefficient and Sentinel-2 (S2) normalized difference vegetation index (NDVI) to develop a near real-time approach for retrieving irrigation timing across various crop fields in France and Spain. Their approach involves a change detection methodology that analyzes two consecutive S1 observations to identify irrigation. According to the findings, the proposed method successfully identified irrigation events that took place over the agricultural plots with an overall accuracy of 84% approximately. However, the ability to detect irrigation events from SAR data mainly depends on the revisit time and the radar wavelength (SAR characteristics) as well as on the vegetation cover (crop type, and growing phase) (le Page et al., 2020). The detection of irrigation events could be hampered by too large revisit times due to the quick dry-up of soil surface 2–3 days after irrigation, leading to water content values similar to those before irrigation (El Hajj et al., 2014). Moreover, El Hajj et al. (2019) have shown that, over cereal crops and grasslands, the usually used (C-band) SAR data could present some limits for estimating soil moisture, due to the low penetration of the signal under well-developed vegetation covers. This pleads for the forthcoming use of L-band data (lower frequency, longer wavelength, and better penetration) for future applications.

On the other hand, optical images have been extensively used to map irrigated areas, based on the difference between the spectral reflectance of irrigated and that of non-irrigated crops, at least in the crop growth periods (Dheeravath et al., 2010; Ozdogan and Gutman, 2008; Pageot et al., 2020) and mainly for cereals. This approach relies on the spectral characteristics of the crops, related to the greenness and healthiness of the leaves that allegedly differ between irrigated and non-irrigated crops. The interpretation of several optical vegetation indices such as the NDVI (Ambika et al., 2016), the normalized difference water index (NDWI) (Deines et al., 2017) or the greenness index (GI) (Chen et al., 2018), has proven to be suitable to investigate the difference in the spectral characteristics of the crops. Despite the high availability of optical data with spatial and temporal resolutions suitable for irrigation monitoring, specifically S2 data, few studies have assessed the potential of optical vegetation indices for detecting irrigation events (dates and doses). Chen et al. (2018) proposed a new approach to monitoring irrigation using MODIS (moderate resolution imaging spectro-radiometer) time series in combination with Landsat images with 30-m spatial resolution. In their study, the irrigation detection approach consisted of counting the possible water supplementations through a threshold-based model based on greenness index (GI) values. Their method showed promising results with an overall detection accuracy of 87%. Even with the interesting revisit time and spatial resolution of the new satellites (5 days and 10 m for S2) the presence of clouds could restrict the use of optical data for irrigation monitoring and mapping, at least when using optical data only.

Over the last 30 years, crop growth models have shown great potential as a valuable and powerful tool to assess agronomical needs and traits (e.g. crop water requirements; biomass, and crop yield), which makes them suitable for crop development monitoring (Garrison et al., 1999; Hook, 1994; López-Cedrón et al., 2008). A crop growth model is most often a set of equations that simulate plant physiological processes and growth (leaves, roots, and fruits), typically at a daily time step (A and Maitra, 2018), as well as the interaction between the “soil-plant-atmosphere-management” (Hoogenboom, 2000; Wallach et al., 2018), in order to estimate crop yield, based on different soil and crop

properties, irrigation management practices and climatic conditions (Brisson et al., 2003; Jones et al., 2003). These multidisciplinary approaches to crop modeling have led to the development of refined and updated crop models, such as WOFOST (de Wit et al., 2019), DSSAT (Hoogenboom et al., 2019), APSIM (Holzworth et al., 2014), AQUACROP (Steduto et al., 2009), STICS (Brisson et al., 2003) or CropSyst (Stöckle et al., 2003). For instance, Hsiao et al. (2009) conducted a study to parameterize and test AquaCrop using data collected at the University of California Davis. The results showed that AquaCrop was able to properly simulate the canopy cover, biomass development, and grain yield of four maize cultivars over six different crop seasons differing in plant density, planting date, and atmospheric evaporative demand, with irrigation treatments that withheld the water up to tasseling, from tasseling onward, intermittently, or completely, under conditions of little rainfall but with the soil at or near field capacity at planting time. In addition to crop yield predictions, crop models can also be used to evaluate crop water requirements or to determine the optimum irrigation management strategies (Guerra et al., 2007; Nijbroek et al., 2003) possibly in support of public policies. Even though, crop modeling applications mostly focused on crop yield predictions (Hoogenboom, 2000; Jones et al., 2003, 1998) with significant variability in accuracy and robustness between models (Palosuo et al., 2011; Rötter et al., 2012). A Crop growth model, such as Optirrig, is a set of equations that simulate plant physiological processes and growth (leaves, roots, and fruits), typically at a daily time step, (A and Maitra, 2018) in order to estimate crop yields, based on different soil properties, crop management practices and climatic conditions (Brisson et al., 2003; Cheviron et al., 2016; Jones et al., 2003). Therefore, crop models are considered powerful tools to define crop water requirements and optimize irrigation management strategies (Guerra et al., 2007; Nijbroek et al., 2003). Even if crop models are easily implemented at the field scale where the main soil properties and agricultural practices can be collected from field surveys, their implementation over larger areas is often limited by the availability of input data (Courault et al., 2021). Thus, uncertainties in estimations of daily or seasonal model variables (soil water reserve, crop development, biomass accumulation, and final yield) are often related to the lack of knowledge about soil characteristics and crop management practices over large areas (Cheviron et al., 2016; Jin et al., 2018; Mailhol et al., 2011). In order to overcome these uncertainties, various studies have incorporated information derived from remote sensing (Claverie et al., 2012; Courault et al., 2021, 2010; Fieuzal et al., 2011; Huang et al., 2016; Kang and Özdoğan, 2019).

These limitations hopefully fall when combining the use of remote sensing data and that of a crop model, which has a high potential to monitor the use of water resources at the field and regional scale (Bastiaansen et al., 2000; Saadi et al., 2015; Toureiro et al., 2017; Yao et al., 2015). The addition of remote sensing data can also improve the estimation accuracy of crop yields in regional studies conducted on sugar beet (Bouman, 1995; Guéris and Duke, 2000), winter wheat (Curnel et al., 2011; Dente et al., 2008; Huang et al., 2015; Jongschaap and Schouten, 2005) and maize (Maas, 1988; Wang et al., 2013). For example, Jongschaap and Schouten (2005) reported that the simulated regional wheat production, by integrating into the ROTASK model the flowering date estimated from remote sensing data, was in agreement with agricultural statistics and that the wheat area could be estimated with an overall users' accuracy of more than 80%.

In coherence, Duchemin et al. (2015) have demonstrated that coupling optical data with a crop growth model allowed better performances for yield and biomass predictions, thanks to the higher precision in the simulation of the crop water requirements and soil water content through the soil water budget part of the model. Battude et al. (2017) developed a model based on the green area index (GAI) and green cover fraction (FCOVER) data, derived from high spatial and temporal resolution optical images, combined with a crop model coupling the Simple Algorithm For Yield estimates (SAFY, (Battude et al., 2016; Duchemin et al., 2008)) to a water balance model adapted from the FAO-56 method

(Allen et al., 1998). The coupled model was used to estimate the dynamics of actual crop evapotranspiration (AET) and retrieve the irrigation amounts on maize plots in the Southwest of France. This allowed us to obtain good estimations for AET ($R=0.88$ and $RRMSE=20\%$) as well as for the total irrigation amounts applied over the maize fields ($R=0.79$ and $RRMSE=18.8\%$). In fact, LAI estimated from remote sensing data was mainly incorporated as a state variable into crop models (Bouman, 1995; Clevers et al., 2002; Courault et al., 2021; Hadria et al., 2006; Huang et al., 2001; Schneider, 2003; Thorp et al., 2010; Tripathy et al., 2013; Yao et al., 2015). For instance, Ines et al. (2013) assimilated remotely sensed MODIS LAI products into the DSSAT-CSM-Maize, using the Ensemble Kalman filter) for maize yield estimation. The results showed that the assimilation of LAI improved the performance by decreasing the root mean squared error (RMSE) of yield estimates by 1.1 t/ha (RMSE decreased from 4.7 to 2.9 t/ha). In addition, Courault et al. (2021) used a spatially-distributed version of the STICS crop model (Brisson et al., 2003) along with daily interpolated Leaf Area Index (LAI) values derived from S2 and acquired over rice fields and assimilated in the model via a forcing mechanism, to evaluate the potential of optical images in combined approaches for monitoring rice cropping systems and yield at farm scale and larger scales. Their results have shown that the assimilation of S2 data significantly improved the plot-scale yield estimation and provided useful information on the spatial variability of yields at the regional scale. Those findings demonstrate that the phenology information provided by canopy state variables, such as LAI, controls crop matter distribution during the growth process, which makes it a valuable indicator of crop water status and thus essential for all crop growth models. In addition, LAI derived from optical remote sensing has greatly improved the ability to monitor crop growth and development at regional and field scales (Chrysaftis et al., 2020; Clevers et al., 2017; Zheng and Moskal, 2009). In fact, irrigation and water stress influence greatly crop development and growth and, consequently, biophysical parameters derived from optical remote sensing such as LAI (Ban et al., 2019; Han et al., 2021; Pôças et al., 2015). Hence, several studies have demonstrated the potential of using LAI derived from Sentinel-2 data as a valuable index of crop irrigation requirements and water stress (Jin et al., 2020; Tewes et al., 2020; Zhuo et al., 2019). Therefore, the key point of the integration of remote sensing-derived biophysical parameters in crop modeling for irrigation detection and optimization applications is to determine how sensitive the crop growth-related outputs of a crop model, such as LAI, are to changes in irrigation levels and water stress. Dynamic crop models that are process-based and integrate a water balance and evapotranspiration components (e.g. AquaCrop (Steduto et al., 2009), STICS (Brisson et al., 2003), SAFYE (Duchemin et al., 2005), Optirrig (Cheviron et al., 2016)) have shown great ability to monitor the effect of water application and stress on plant growth and simulate the crop response to irrigation water (Castañeda-Vera et al., 2015; Duchemin et al., 2008; Mailhol et al., 2018; Silvestro et al., 2017; Varella et al., 2012). For instance, Mailhol et al. (2011) conducted a study over irrigated maize plots to analyze the potential of the PILOTE model (the agronomic and the hydrological core of the Optirrig) for crop development and yield prediction. The model allowed satisfactory simulations and prediction of the soil water balance and LAI along the cropping cycle. In fact, PILOTE simulates soil water balance and crop yield at a daily time step by the association of a soil module and a crop module that is based on the LAI simulation and its response to water stress and soil available water. In addition, Varella et al. (2012) applied a global sensitivity analysis on the input parameters of the STICS model in order to determine the importance of different soil parameters. The LAI have shown unique high sensitivity to the initial soil water content and the water content at field capacity at the stage of maximum leaf growth rate and flowering stage of the crop cycle, respectively. Therefore, incorporating the information derived from remotely-sensed LAI in crop models using simple assimilation methods, such as forcing methods, has great potential in providing valuable information about crop transpiration and water stress and therefore

assessing crop response to several agricultural practices, especially irrigation (Jin et al., 2018; Silvestro et al., 2017).

Although operational objectives of regional-scale supervision would certainly require the use of both radar and optical data, in combination with a crop model, this paper focuses on "how far can we go by resorting to LAI data only?". The crop model used here is the Optirrig model (Cheviron et al., 2016; Cheviron et al., 2020) for the simulation, analysis, and optimization of irrigation scenarios. The assigned exploratory objective to Optirrig is the identification of the real series of irrigation events (dates and amounts) for several irrigated maize fields in the Occitanie region in Southeast France. The method is based on an inversion approach that seeks the irrigation events that minimize the difference between the LAI values derived from optical images and the LAI values simulated by Optirrig, at the dates of available S2 observations. First, synthetic experiments were performed to assess the impact of S2 revisit time (time lag between two cloud-free images) and the error on LAI, derived from optical images, using noisy LAI values mimicking the error on S2 observations. Second, daily interpolated LAI values derived from S2 are used. The performance of the proposed irrigation detection approach is reported and assessed based on the real and the detected irrigation dates and amounts applied over the studied maize plots.

2. Material and method

2.1. Study sites

In this study, two different irrigation sites are selected in the Occitanie region (Southern France). The first one is an experimental field, located in the Northern part of Montpellier, in the south-east of France and the second one is near Tarbes, in the south-west of France (Fig. 1). Montpellier finds itself in a zone with typically Mediterranean climatic conditions characterized by a warm and temperate climate (average

annual temperature of 15.0 °C). The average annual precipitation is 629 mm and rainfall mostly occurs in winter.

By contrast, the climate in Tarbes is humid to oceanic with an average annual precipitation of 1200 mm. The summer season is much more humid than in Montpellier with an average precipitation of 300 mm from June to September. However, in both regions, irrigation mainly occurs in the summer season, usually starting in June and ending in September, depending on local conditions. Field trials were conducted in three reference plots (described in Section 2.2), the M1 plot in 2017 in Montpellier then the M2 and M3 plots near Tarbes, in 2019 and 2020, respectively (Fig. 1).

The Occitanie region is an important agricultural area where various cereals and spring/summer vegetables are cultivated. The most cultivated cereals in Occitanie (maize, soybean, wheat, barley, and sunflower) represent 34% of the whole cultivated area in the region, according to the agricultural Land Parcel Information System provided by the French Services and Payments Agency (Cantelaube and Carles, 2015). Coping with low and very variable rain amounts, recurrent water stress, and also heat stress are the main challenges for cereal growers in the region, considering irrigation as insurance to obtain enough yield but facing the issue of limited resource availability.

2.2. Site management and meteorological data

For an overview, the total number of irrigation events is given in Table 1 for each plot, together with sowing and harvest dates. In Montpellier, the M1 plot is a deep soil of colluvial-alluvial origin. Its texture is silty clay loam (around 24% clay, 44% loam, and 32% sand) which is characterized by an important water-holding capacity (Soil Survey Manual, 2017). Near Tarbes, the M2 and M3 plots are of silt loam texture with high fertility and significant drainage capacity (Kettler et al., 2001).

Air temperature (Tmin, and Tmax), solar radiation (Rs), rainfall (R),

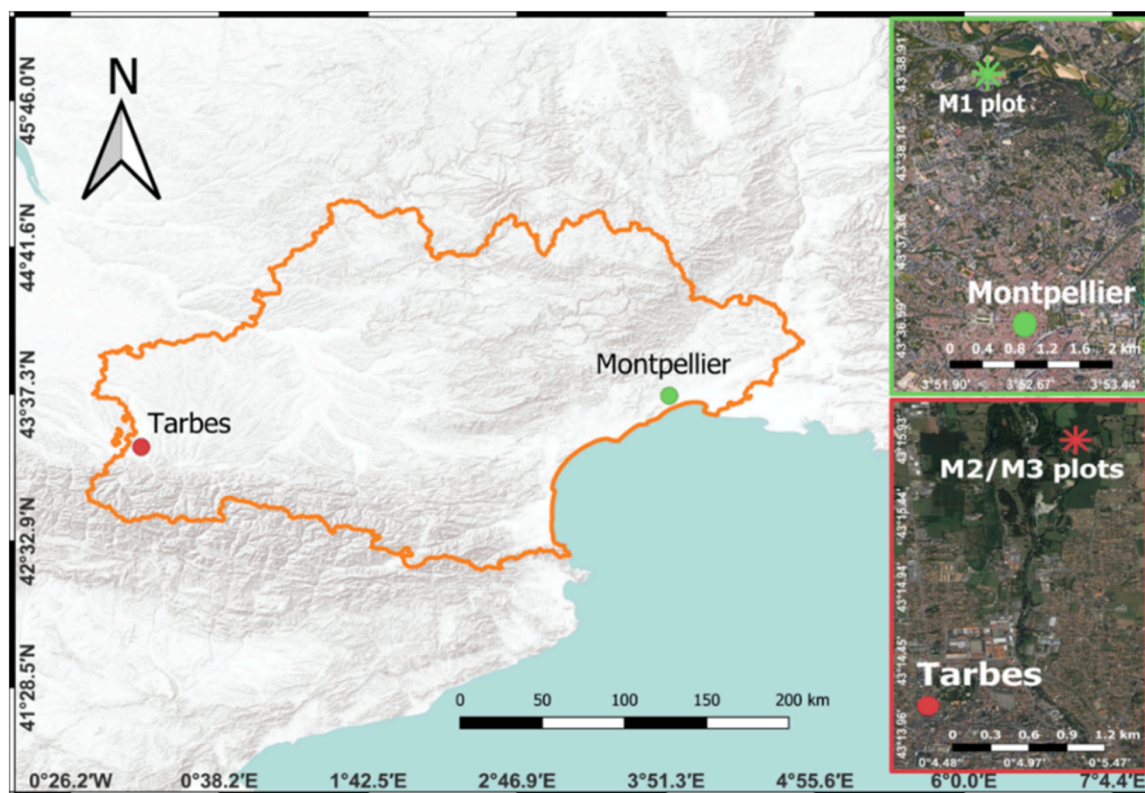


Fig. 1. Location of the two study Sites in France. The Occitanie region is outlined in orange. The three experimental maize plots in Montpellier in 2017 (M1) and Tarbes in 2019 (M2) and 2020 (M3) are shown on the right.

Table 1
Summary of experimental maize plots' irrigation and crop management practices.

Region	Year	Plot	Number of irrigations	Sowing date	Period of irrigation	Harvest date	Irrigation method
Montpellier	2017	M1	10	15 April	28 June – 8 August	25 September	Sprinkler (Raingun)
Tarbes	2019	M2	4	01 May	1 July – 29 July	01 October	Sprinkler (Raingun)
Tarbes	2020	M3	3	08 May	9 July – 6 August	30 September	Sprinkler (Raingun)

and Penman-Monteith reference evapotranspiration (ET_0), were collected on site (Table 2).

Fig. 2 shows daily average air temperature (T_{avg} in °C), Penman-Monteith reference evapotranspiration (ET_0 in mm), and rainfall (R in mm) in the three experimental plots, M1, M2, and M3, over the days after seeding (DAS).

2.3. Optirrig model description

Optirrig is a crop growth and irrigation model composed of an inner module in charge of the hydrological and agronomical calculations, and an outer module that deals with the generation, analysis and optimization of irrigation scenarios. Optirrig takes most of its agronomic part from adaptations of the former Pilote model (Mailhol et al., 2011, 1997) developed within the same research team. Optirrig simulates crop growth and yield as a function of water and nutrients availability and consumption, focusing on the identification of relevant irrigation and fertilization practices and decision rules (see Cheviron et al., 2016), mainly over cereals and horticulture. The model version used here is the one devoted to field crops, whose conceptual scheme appears in Fig. 3. No nitrogen stress is assumed to occur since fertilization was sufficient on the study sites: the nitrogen cycle part of the model is therefore not shown.

In its inner hydro-agronomic module, Optirrig performs a daily water balance that encompasses infiltration and drainage, evaporation and transpiration, and changes in soil water reserves (R_1 , R_2 , R_3) in the surface, root-zone, and deep reservoirs, respectively. Optirrig requires four daily climatic forcings: precipitations (P), mean air temperature (T), potential evapotranspiration (ET_0), and total global solar radiation (R_g). In addition, irrigation (I) could be required for Optirrig as a management forcing parameter. Crop growth is followed through the dynamics of the Leaf Area Index (LAI) which is predicted from thermal time (TT) and possibly hampered by water stresses (S_w), illustrated in Fig. 3. The crop coefficient (K_c) and partition coefficient (C_p) are calculated from LAI as the vegetal cover is known to govern the partition

of ET_0 into transpiration demand (T_{p0}) and evaporation demand (E_{s0}). The actual transpiration (T_p) and evaporation (E_s) amounts are then calculated from the available water reserves, whose values are then updated. Biomass accumulation (TDM) is calculated from radiation interception and is also possibly affected by water stresses. Finally, crop yield (Y) is evaluated through the harvest index (HI) whose value differs from a potential value if the chronicle of LAI values throughout the cropping season denotes significant water stresses. Table 3 adds more details, especially on the soil and crop parameters involved.

In its outer layer, Optirrig enables the generation and analysis of multiple irrigation scenarios for water efficiency improvement and yield optimization purposes. The model's structure also provides the possibility to use independent information (regarded as observations) on some of the state variables, for various classical (e.g. model fitting) or exploratory purposes. Here, the LAI values obtained from remote sensing will be compared to the predicted LAI values, seeking the irrigation dates and doses that close the gap between observations and predictions.

2.4. Sentinel-2 data

Numerous cloud-free optical images of Sentinel-2 (S2) were available throughout the cropping seasons of 2017, 2019, and 2020: 15 images on the M1 plot, 21 on the M2 plot, and 17 on the M3 plot, yielding as many "observed" LAI values. The images were downloaded for each study site via the Theia website (<https://www.theia-land.fr/>) which provides S2 images corrected for atmospheric effects through the Level-2A operational processor that uses algorithms of scene classification and atmospheric correction, described by Hagolle et al. (2018).

The LAI values obtained from S2 (LAI_{S2}) were derived using the built-in Biophysical processor, also called Sentinel-2 Level 2 Prototype Processor (SL2P) within the Sentinel Application Platform (SNAP). The Biophysical processor behind the SL2P is the Sentinel-2 Toolbox (S2Tbx), developed by Weiss and Baret (2016). The S2Tbx uses eight reflectance bands (B3, B4, B5, B6, B7, B8A, B11, and B12), using

Table 2
Monthly climatic data for the maize experimental plots, M1 in Montpellier, and M2 and M3 in Tarbes: Minimal and maximal air temperature (T_{min} , and T_{max} in °C), daily averaged values of R_s (Avg- R_s in $MJm^{-2}d^{-1}$), rainfall (R in mm/month) and Penman-Monteith reference evapotranspiration (ET_0 in mm/month).

Plot	Year	Month	T_{min} (°C)	T_{max} (°C)	Avg- R_s ($MJm^{-2}d^{-1}$)	R (mm/month)	ET_0 (mm/month)
M1	2017	April	9.5	17.6	20.75	39.5	93.7
		May	11.3	23.1	24.1	27.4	131.2
		June	18.7	28.7	25.97	73.2	166.3
		July	20.1	28.3	26.06	4.7	182.2
		August	19.7	30.9	20.84	8.9	145.1
M2	2019	September	13.8	23.6	16.31	6.5	93.9
		May	0.7	26.3	20.3	117.8	104.3
		June	6.8	35.4	22.1	65.6	127.9
		July	10.9	36.6	21.2	100.8	133.4
		August	9.6	32	18.8	119	109.2
M3	2020	September	6.4	29.3	16.5	57.6	78.1
		October	5.1	31.4	9.5	91.6	37.8
		April	1.1	23.7	15.6	159.2	78.2
		May	9.3	29	21.5	77.6	120.6
		June	8	31.6	19.1	100.6	111.1
		July	11.2	36.1	20.8	11.8	127.8
		August	9.1	36.2	18.9	62.2	110.2
		September	4.8	33.7	15.7	101	80.5

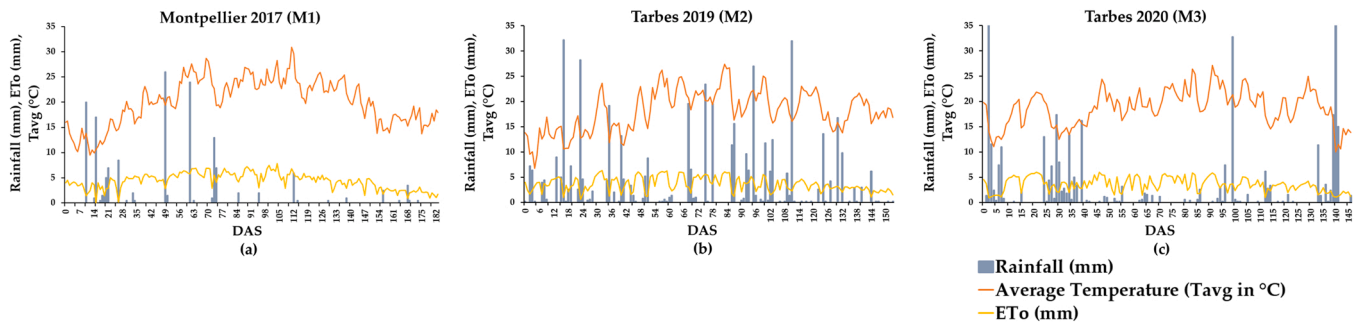


Fig. 2. Daily average air temperature (T_{avg} in $^{\circ}\text{C}$), Penman-Monteith reference evapotranspiration (ET_0 in mm) and rainfall (R in mm) during the crop growing cycle of maize: (a) Montpellier in 2017 (M1), (b) Tarbes in 2019 (M2) and (c) Tarbes in 2020 (M3).

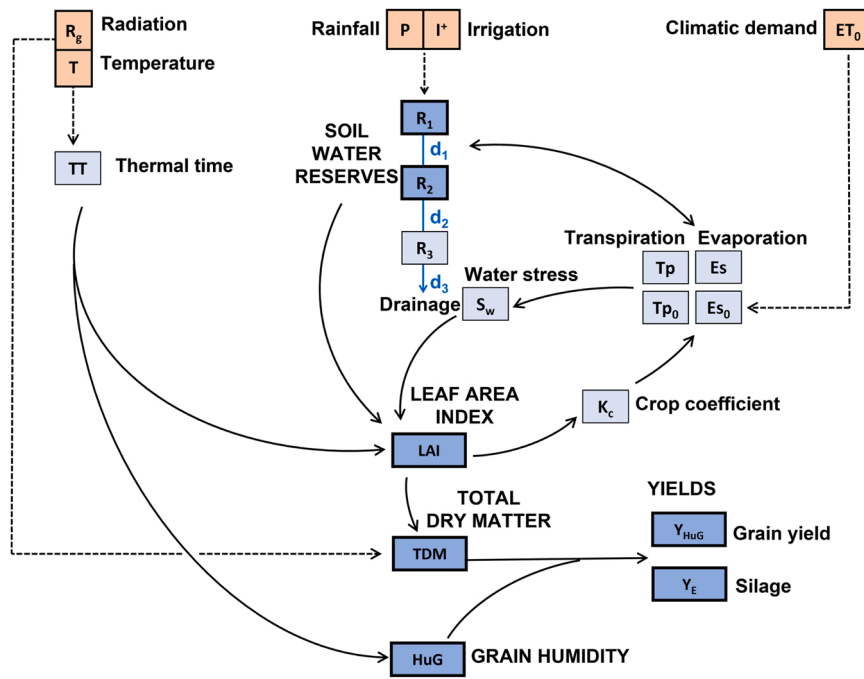


Fig. 3. Conceptual scheme of the Optirrig model, showing the organization of climatic forcings (orange squares), intermediate variables (light blue squares) and key state variables (grey sketches with thick contours: LAI, TDM and Y). Irrigation is noted I^+ to indicate that this model forcing depends on multiple management options and associated parameters.

radiative transfer models (RTMs), i.e., PROSAIL and Neural Networks algorithm. The LAI values for all pixels were averaged, at the plot scale, for each S2 date. The time period between two consecutive S2 images varied between 5 and 20 days, depending on the plots. In addition to the “observed S2” LAI values, interpolated LAI values (LAI_{int}) were generated, following a double logistic fitting technique (Fisher et al., 2006), between any two successive LAI_{S2} values (Fig. 4).

2.5. Irrigation retrieval approach

Our approach aims to retrieve irrigation timing and amounts at the plot scale based on the integration of LAI data derived from Sentinel-2 (LAI_{S2}) into Optirrig through an inversion technique. Thus, irrigation events were estimated by comparing LAI_{S2} to the LAI simulated by Optirrig through the injection of several combinations of irrigation timings and amounts (irrigation combination) applied between two eventual Sentinel-2 images. The irrigation combination that minimizes the difference between the simulated LAI (Optirrig) and the observed LAI (derived from S2) is considered the most probable.

In order to assess the impact of the frequency of S2 observations and the window length between two consecutive S2 images ($\Delta S2$ in days)

and the errors on the LAI_{S2} , synthetic experiments were designed and conducted. Several $\Delta S2$ will be investigated (described in Section 2.6) and our approach will be tested considering each time length between two consecutive synthetic S2 acquisition dates, $t_{(i-1)}$ and $t_{(i)}$.

Therefore, the irrigation (date and amount) retrieval approach is summarized in Fig. 5 and implemented in eight steps:

- Step 1** - Simulate in Optirrig the LAI time series ($LAI_{(i)}$ at $t_{(i)}$) based on growing conditions (weather and soil conditions) and management practices (with irrigation) similar to those that occurred over the three experimental plots (M1, M2 and M3).
- Step 2** - Generate in Optirrig LAI values at each $t_{(i)}$ that are computed when no irrigation ($LAI_{0(i)}$, rainfed) occurred between $t_{(i-1)}$ and $t_{(i)}$, in order to investigate the effect of irrigation water applied on the LAI.
- Step 3** - Add noise to the simulated $LAI_{(i)}$ (see Section 2.5.2) in order to make the simulated data approximately closer to real S2 data and to account for the error in the S2 observations. Thus, a vector $\vec{LAI}_{(i)}$ at each $t_{(i)}$ represents the noisy $LAI_{(i)}$ values.

Table 3

List of main source data required to run the model, with their associated category, code, name, description, reference value, and range tested in sensitivity analysis and units. Data have been sorted into the Parameters: Plant, Soil, Temperature, and Management controls categories; Variables: Crop development and water budget variables. The reference values that pertain to maize, under sprinkler irrigation, on the studied sites are listed in Montpellier and Tarbes columns.

Category	Name	Description	Montpellier (M1)	Tarbes (M2/M3)	Range	Unit	
Parameters	Temperature	T_i	Temperature sum for root installation	150	150	±7.5%	C
		T_m	Temperature sum to reach the maximum LAI	1300	1300	±5%	C
		T_{mat}	Temperature sum for crop maturity	2050	2050	±5%	C
		T_s	Temperature sum for crop emergence	100	100	±10%	C
		T_{s1}	Temperature sum for the 1st critical stage	900	900	±10%	C
		T_{s2}	Temperature sum for the 2nd critical stage	1700	1700	±10%	C
	Soil	K_{ru}	Easily usable reserve/field capacity	0.66	0.68	±7.5%	-
		P_{max}	Maximum profile and rooting depth	1.20	1.10	±7.5%	m
		V_r	Root growth rate	1.50	1.50	±10%	cm.d ⁻¹
		θ_{fc}	Field capacity	0.29	0.26	±7.5%	-
		θ_{wp}	Wilting point	0.12	0.10	±7.5%	-
		a_w	Controls the decrease of HI for low LAI values	0.12	0.12	±10%	-
	Plant	HI_{pot}	Potential Harvest index (HI)	0.52	0.52	±7.5%	-
		K_{cmax}	Maximum value for crop coefficient (K_c)	1.20	1.20	±10%	-
		LAI_{max}	Maximum LAI value	5.00	4.50	±7.5%	-
		LAI_{opt}	Supposed HI-optimal LAI value	2.50	2.50	±10%	-
		G_{hu}	Percentage of grain humidity	15	15	±33%	-
		RUE	Radiation Use Efficiency	1.35	1.35	±7.5%	-
		α_1	First shape parameter for LAI curves	2.50	2.50	±15%	-
		α_2	Second shape parameter for LAI curves	1.00	1.00	±15%	-
β		Third shape parameter for LAI curves	2.50	2.50	±15%	-	
λ		Harmfulness of the water stress	1.25	1.10	±10%	-	
Management	-	Irrigation dose (applied at each irrigation)	30	40	20–40	mm	
	-	Dose applied at sowing	30	40	25–35	mm	
	-	Soil reserve when starting the simulation	300	500	Fixed	mm	
	-	Period allowed for irrigation (in days after sowing)	140	115	120–160	-	
	-	Mulch effect	0	0	0–1	-	
	-	Sowing day	105	121	104–124	-	
	-	Water reserve Ratio that triggers irrigation	70	68	53–72	%	
Variables	Crop development	TT	Sum of Temperature	-	-	0.0–2250.0	C
		K_c	Crop coefficient	-	-	0.0–1.0	-
		C_p	Partition crop coefficient	-	-	0.0–0.85	-
		T_p	Crop Transpiration	-	-	0.0–8.5	mm.d ⁻¹
		Tp_0	Potential crop Transpiration	-	-	0.0–9.6	mm.d ⁻¹
	Water budget	HI	Harvest index	-	-	0.4–0.61	-
		R_1	Water reservoir of the first soil layer	-	-	4.0–30.0	mm
		R_2	Water reservoir of the second soil layer	-	-	45.0–204.0	mm
		R_3	Water reservoir of the third soil layer	-	-	0.0–206.0	mm
		S_w^s	Water stress index	-	-	0.0–1.0	-
Es	Evaporation	-	-	0.0–1.9	mm.d ⁻¹		
Es_0	Potential Evaporation	-	-	0.2–2.5	mm.d ⁻¹		

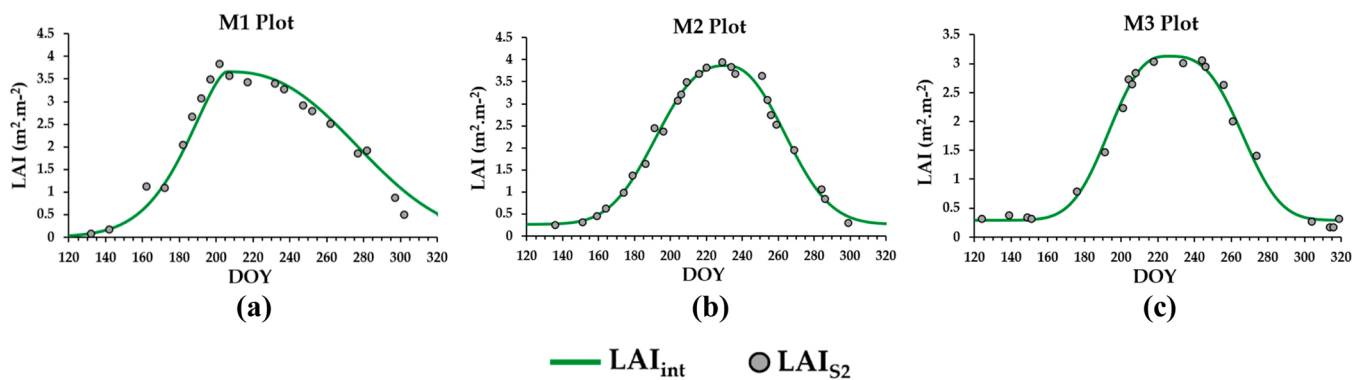


Fig. 4. LAI_{S2} values (grey dots) derived from Sentinel-2 optical images and LAI_{int} curves (green lines) obtained by double sigmoid smoothing, in the M1 plot (a), M2 plot (b) and M3 plot (c).

- Step 4** - Filter the outliers of $\overline{LAI}_{(i)}$ following the two deviations approach described in the Section 3.2.
- Step 5** - Calculate the minimal and maximal difference ($G_{\min(i)}$ and $G_{\max(i)}$) between the noisy LAI values and $LAI_{0(i)}$ at each $t_{(i)}$.
- Step 6** - Inject into Optirrig all possible irrigation scenarios as combinations of different dates (j is the irrigation date in day; at $t_{(i)}, j$

- is between (i) and $(i - 1)$) and doses (k) ($C_{(j,k)}$) between two consecutive $S2$ images and compute the difference $G_{(j,k)}$ between the simulated $LAI_{(j,k)}$ and $LAI_{0(i)}$.
- Step 7** - Calculate $\overline{D}_{(j,k)}$ as the difference between $LAI_{(j,k)}$ and $LAI_{(i)}$ in order to identify the closest $C_{(j,k)}$ to reality through a function of minimization.

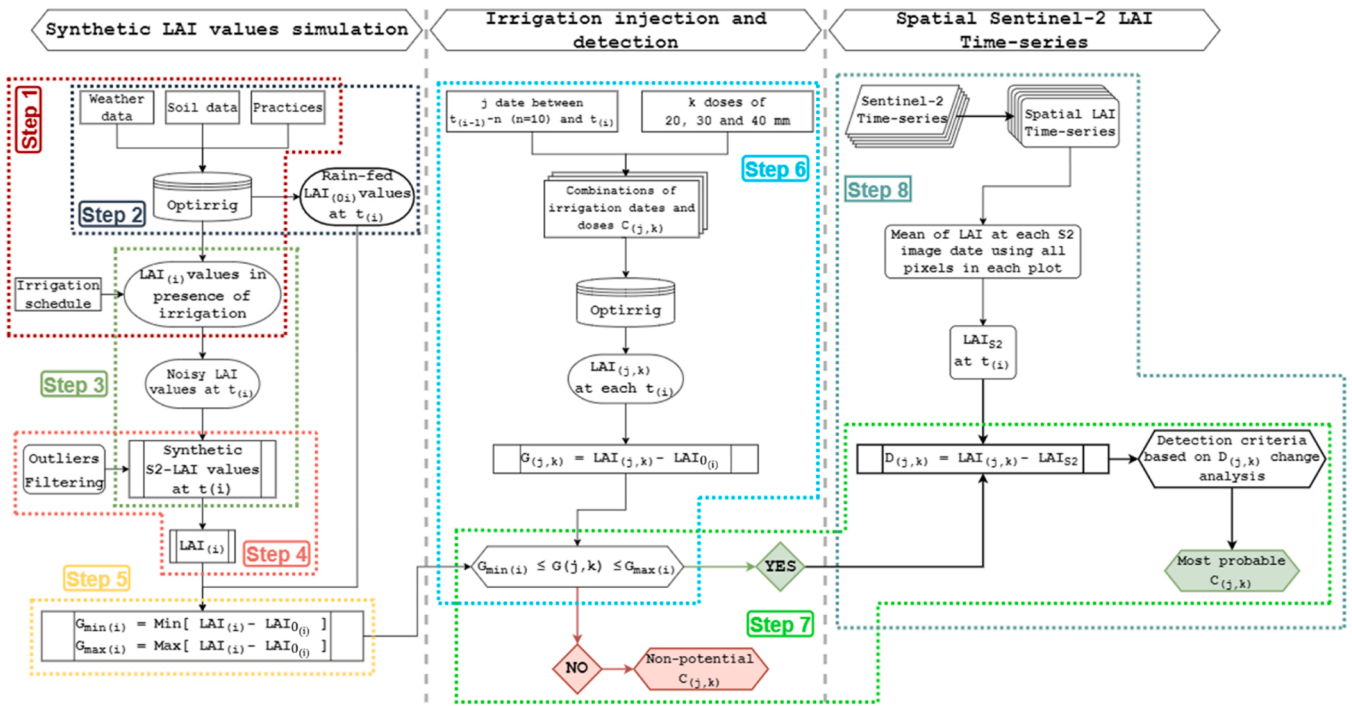


Fig. 5. Workflow overview describing the different steps of simulations to assess the irrigation dates and amounts retrieval approach. $\overline{LAI}_{(i)}$ represents the noisy $LAI_{(i)}$ values. The dashed colored lines refer to the eight steps of the irrigation retrieval approach listed in Section 2.5: Step (1) in burgundy; Step (2) in navy blue; Step (3) in dark green; Step (4) in brick dark pink; Step (5) in yellow; Step (6) in cyan; Step (7) in light green and Step (8) in light blue grey. The different forms represent the forcing data (rectangles with thick contours), Sentinel-2 data (rectangles with rounded contour), Optirrig simulated LAI data (oval), Sentinel-2 Time series (trapeze), criteria and conditions (hexagon) and the vectors (rectangles with two vertical lines).

8. Step 8 - Evaluate the approach using real S2 LAI data (LAI_{S2}).

2.5.1. LAI time series and irrigation dates simulation

Our methodology aims to be generic: in this study, three representative study cases (illustrated by the three experimental plots M1, M2 and M3) are analyzed and may allegedly represent the development of maize in two climatic conditions (Mediterranean context) and irrigation practices (Fig. 6). The first study case is a plot of maize cultivated in Montpellier in 2017 growing season (M1). The climatic and agricultural conditions are typical of a semi-arid region where the frequency of irrigation is high and plants are more susceptible to water stress conditions (Fig. 6a). Thus, through Optirrig, irrigation water needs were simulated and seven reference irrigation events (d_R) of 30 mm were applied throughout the season, which corresponds to the irrigation practice and frequency usually applied for maize production in a similar climate and conditions (Montpellier). Fig. 6b and c show the crop development simulated by Optirrig using real irrigation practices and data collected in Tarbes for 2019 (M2) and 2020 (M3) rainy years, leading to lower irrigation frequencies occurrence because of the high

amounts of precipitation and frequency of rainfall events during the maize growing season in Tarbes. In fact, the cumulative rainfall reached 460 mm in 2019 and 362 mm in 2020 for an average of 77 rainfall events per year between May and October of each year. Thus, Optirrig will simulate, on a daily time step, the development of the crop throughout the growing season, for maize under the occurrence of irrigation. Supposing that cloud-free S2 images are highly available with one image every five days ($\Delta S2 = 5$ days), the LAI values derived from S2 integrate the effect of a potential irrigation and rainfall between S2 acquisition dates ($t_{(i)}$). In coherence, Fig. 6 show the simulated LAI values, of irrigated maize, with a time step of five days, $LAI_{(i)}$ at $t_{(i)}$ (green cross signs). Conversely, in an operational context, when no information about the irrigation is available, Optirrig will simulate the LAI under rain-fed conditions ($LAI_{R(i)}$) represented by the red x-signs (Fig. 6). Basically, by comparing the $LAI_{(i)}$ and $LAI_{R(i)}$ values, it is noticeable that before the first irrigation the simulations match perfectly, and then, discrepancies are observed after that the irrigation season began, demonstrating that without irrigation data Optirrig will underestimate the LAI. However, the aim of the study is to detect potential irrigations that occurred between two successive S2 images. It is, then, essential

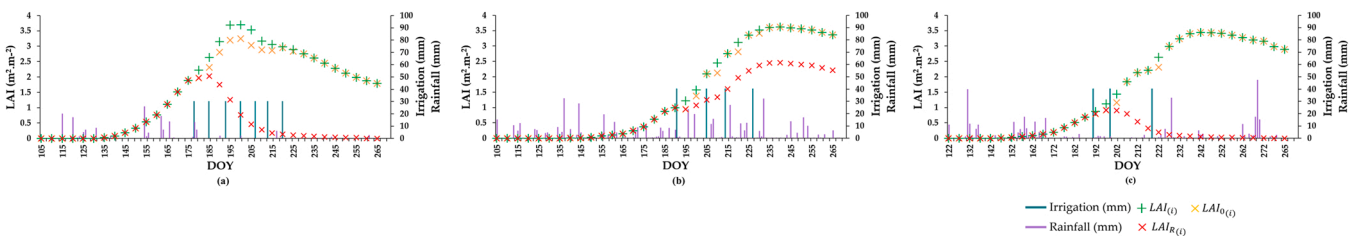


Fig. 6. $LAI_{(i)}$ under irrigated conditions (green cross signs) $LAI_{R(i)}$ under rain-fed conditions (red x-signs) and $LAI_{0(i)}$ (yellow x-signs) under rain-fed conditions "by intervals" simulated by Optirrig for each study case: (a) Montpellier in 2017 (M1), (b) Tarbes in 2019 (M2), (c) Tarbes in 2020 (M3). The blue and violet bars represent the irrigation and rainfall amounts throughout the season, respectively.

that $LAI_{(i)}$ simulations accurately reflect the effects of the occurrence or not of irrigation on the crop between $t_{(i-1)}$ and $t_{(i)}$. Therefore, $LAI_{0(i)}$ values are simulated, at each date $t_{(i)}$, considering that no irrigation occurred between two consecutive S2 images, $t_{(i-1)}$ and $t_{(i)}$ (yellow x-signs), in order to quantify the effect of the absence of an irrigation water supply that possibly occurred between $t_{(i-1)}$ and $t_{(i)}$ (S2 acquisition dates) on the $LAI_{(i)}$. This way we can define the irrigation thanks to this difference which is obviously a forecast of irrigation water supply. In other words, a divergence between the $LAI_{(i)}$ and the simulated $LAI_{0(i)}$ (not integrating irrigation) is an indirect proof of irrigation occurrence between $t_{(i-1)}$ and $t_{(i)}$. Conversely, no discrepancy observed means the absence of irrigation or/and the low effect of irrigation applied on vegetative growth as seen in Fig. 6, especially at early (before the irrigation season) and later stages (after the vegetative cycle) of the growing season.

2.5.2. Synthetic S2 derived LAI data

In order to convey more realistic values and better approximates to the real Sentinel-2 LAI data, an error corresponding to the accuracy of the LAI observations was added to each simulated $LAI_{(i)}$ value, at the $t_{(i)}$ date. This error varies with the value of the LAI obtained from S2 data at the same date and is estimated as follows (Weiss and Baret, 2016):

$$\alpha LAI_{(i)} = \max(\sigma_0, LAI_{(i)} \times \sigma_R) \quad (1)$$

where $\alpha LAI_{(i)}$ is the absolute error on LAI, $\sigma_0 = 0.3$ and $\sigma_R = 0.2$.

Accordingly, for $LAI_{(i)}$ at each date of S2 acquisition $t_{(i)}$, 10,000 noise samples (NS) were randomly selected from the zero-mean Gaussian noise distribution with a standard deviation of $\pm \alpha LAI_{(i)}$. To filter the outliers of NS at each date, the random draws located at more than two deviations on either side of the median value have been excluded. This requires an estimate of the standard deviation of the distribution that is not presenting outliers (Leys et al., 2013). The deviation is estimated at each $t_{(i)}$ as follows from successive stages:

1. Calculate the median M of all the NS:

$$M = \text{median}(NS) \quad (2)$$

2. Calculate the absolute deviations of NS from the median M:

$$AD = \text{abs}(NS - M) \quad (3)$$

3. Calculate MAD, the median of the absolute deviations:

$$MAD = \text{median}(AD) \quad (4)$$

4. Evaluate the sought standard deviation from the MAD value:

$$\sigma = 1.4826MAD \quad (5)$$

Finally, only NS within the $[M - 2\sigma; M + 2\sigma]$ range are used, to create the \overrightarrow{LAI}_i vector of noisy $LAI_{(i)}$ values, at each $t_{(i)}$, to be compared with the $LAI_{0(i)}$ and $LAI_{(i)}$ values that stand for the simulated LAI values under "rained by interval" and "possibly irrigated" conditions, respectively, as shown in Fig. 7. The difference between the values of \overrightarrow{LAI}_i and $LAI_{0(i)}$ is thought to signal the occurrence of an irrigation between $t_{(i-1)} - n$ and $t_{(i)}$, where $t_{(i-1)} - t_{(i)}$ is the $\Delta S2$ the interval of days between two consecutive S2 images and n days before. The value of n, which will be discussed later, represents the number of days where water stress can affect the LAI.

This difference is a vector, noted \vec{G}_i :

$$\vec{G}_i = \overrightarrow{LAI}_i - LAI_{0(i)} \quad (6)$$

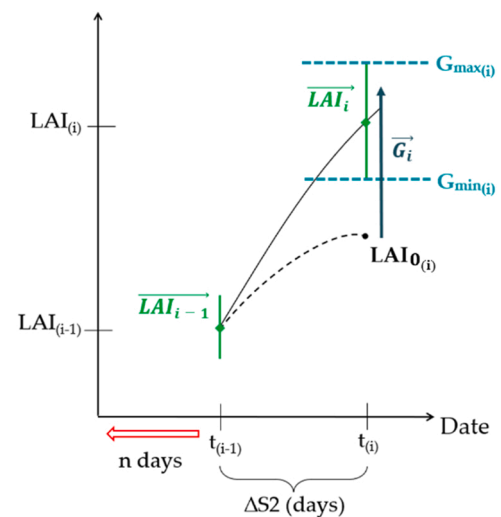


Fig. 7. Calculation scheme for the $G_{\min(i)}$ and $G_{\max(i)}$ values, relying on the vector of differences \vec{G}_i between the noisy \overrightarrow{LAI}_i values and the simulated "rained by interval" $LAI_{0(i)}$ value, over the $\Delta S2$ interval of days between two consecutive S2 images at dates $t_{(i-1)}$ and $t_{(i)}$. The irrigation events responsible for the \vec{G}_i values will be sought backwards from the $t_{(i)}$ date and until the $t_{(i-1)} - n$ date.

The maximum and minimum values of \vec{G}_i at $t_{(i)}$ are:

$$G_{\min(i)} = \text{Min}[\overrightarrow{LAI}_i - LAI_{0(i)}] \quad (7)$$

$$G_{\max(i)} = \text{Max}[\overrightarrow{LAI}_i - LAI_{0(i)}] \quad (8)$$

Based on the reasoning in Section 2.5.1, a divergence between the $LAI_{(i)}$ and $LAI_{0(i)}$ signals the possibility of occurrence of an irrigation between $t_{(i-1)}$ and $t_{(i)}$. However, the $LAI_{0(i)}$ values are compared to the vector of noisy $LAI_{(i)}$ values (\overrightarrow{LAI}_i), due to the error added on the $LAI_{(i)}$. Therefore, the maximum error (maximum NS) added on the $LAI_{(i)}$ has to be minor than the difference between $LAI_{(i)}$ and $LAI_{0(i)}$, in order to maintain a difference between \overrightarrow{LAI}_i and $LAI_{0(i)}$. In other words, in order to detect a possible irrigation between $t_{(i-1)}$ and $t_{(i)}$ the minimum value of the vector \overrightarrow{LAI}_i has to be higher than the $LAI_{0(i)}$ and, thus, verify the condition $G_{\min(i)} > 0$ ($G_{\min(i)} = \text{Min}[\overrightarrow{LAI}_i - LAI_{0(i)}]$). Fig. 8 demonstrates the variation of $G_{\min(i)}$ over the three study cases' growing seasons (M1, M2 and M3). Negative values of $G_{\min(i)}$ mean that the minimum value of \overrightarrow{LAI}_i is minor than $LAI_{0(i)}$ and the effect of an irrigation occurrence is not significant on the values of $LAI_{(i)}$. Conversely, all the noisy $LAI_{(i)}$ in \overrightarrow{LAI}_i show higher values than $LAI_{0(i)}$ when positive $G_{\min(i)}$ are observed and thus, denoting an indirect proof of the irrigation occurrence between $t_{(i-1)}$ and $t_{(i)}$.

2.5.3. Injection and testing of irrigation events in Optirrig

Optirrig assumes the effect of water stress on the LAI dynamics is a damped effect that results from a relative deficit of evapotranspiration over the last 10 days (Cheviron et al., 2016), which suggested taking $n = 10$ in Fig. 7, by security. This means searching for an irrigation event that occurred at the j date between $t_{(i-1)} - 10$ and $t_{(i)}$. As for the possible irrigation amounts, we restrained the set to realistic values, with three possibilities: $k = 20, 30$ or 40 mm. This produces $C_{(j,k)}$ combinations of dates and amounts to test, resulting in $LAI_{(j,k)}$ values simulated by Optirrig (Fig. 10) and therefore in $G_{(j,k)}$ differences with $LAI_{0(i)}$:

$$G_{(j,k)} = LAI_{(j,k)} - LAI_{0(i)} \quad (9)$$

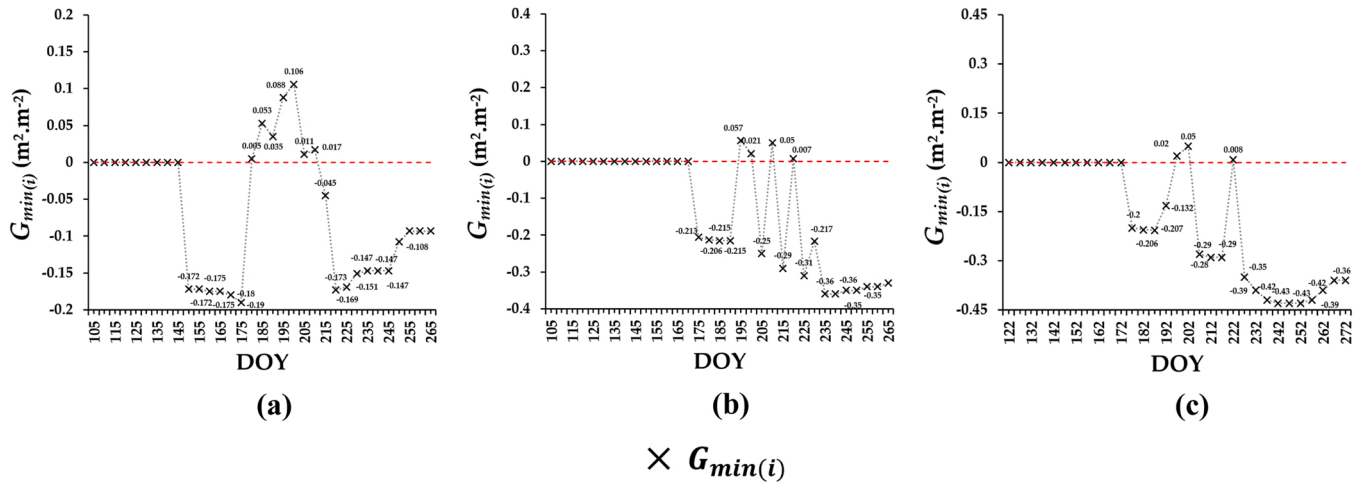


Fig. 8. The calculated $G_{min(i)}$ based on the minimum difference between \overline{LAI}_i and $LAI_{0(i)}$ at $t_{(i)}$ ($G_{min(i)} = \text{Min}[\overline{LAI}_i - LAI_{0(i)}]$) as a function of the day of the year over the maize growing season. (a) Montpellier in 2017 (M1); (b) Tarbes in 2019 (M2); (c) Tarbes in 2020 (M3).

Thus, $G_{(j,k)}$ can be represented in a matrix that illustrates the differences between the $LAI_{(j,k)}$ and $LAI_{0(i)}$ for the $C_{(j,k)}$ injected for different dates and doses of irrigation.

2.5.4. Irrigation detection criteria

In order to retain $C_{(j,k)}$ as a possible irrigation, $G_{(j,k)}$ at $t_{(i)}$ has to verify the following condition:

$$G_{min(i)} \leq G_{(j,k)} \leq G_{max(i)} \quad (10)$$

Conversely, if $G_{(j,k)} < G_{min(i)}$, $LAI_{(j,k)}$ does not fall in the range of \overline{LAI}_i (the noisy $LAI_{(i)}$) so the difference between $LAI_{(j,k)}$ and $LAI_{0(i)}$ is not sufficient to argue that an irrigation has occurred at a date j with a dose k . In complement, if $G_{(j,k)} > G_{max(i)}$, then $LAI_{(j,k)}$ exceeds the assumed range of LAI values ($LAI_{(i)}$), meaning that the hypothesized irrigation would be responsible for a higher LAI value than what is assumed possible.

There may be 0, 1 or several probable (or recognized) irrigation events between the $t_{(i-1)} - n$ and $t_{(i)}$ dates. Further investigation is necessary to evaluate the effect of the combinations of recognized irrigation events. This is done by studying the magnitude of the difference $\overline{D}_{(j,k)}$ between the $LAI_{(j,k)}$ and the observed $LAI_{(i)}$ (Eq. (11)): for an hypothesized $C_{(j,k)}$ irrigation, the highest $\overline{D}_{(j,k)}$ values mean the lowest probability for $C_{(j,k)}$ to have occurred (Fig. 9):

$$\overline{D}_{(j,k)} = LAI_{(j,k)} - LAI_{(i)} \quad (11)$$

The objective of the inversion process is to detect an irrigation date and amount between two S2 images. Thus, we are searching for the injected irrigation $C_{(j,k)}$ that leads to the least $|D_{(j,k)}|$ difference between $LAI_{(j,k)}$ and $LAI_{(i)}$. The result section will show how to formulate four irrigation detection criteria from the change in amplitude and magnitude of the signed $D_{(j,k)}$ difference.

1. C1 criterion. $\overline{D}_{(j,k)}$ switches polarity from positive to negative
2. C2 criterion. $\overline{D}_{(j,k)}$ transitions from zero to negative
3. C3 criterion. $\overline{D}_{(j,k)}$ switches polarity from negative to positive
4. C4 criterion. $\overline{D}_{(j,k)}$ transitions from negative to zero

In order to assess the interval of days between the detected and the reference irrigation date, $|\Delta t|$ (in days) is calculated as the absolute value of difference between the detected date of the irrigation (d_D) and the date of the reference (simulated) or real irrigation (d_R) as follow:

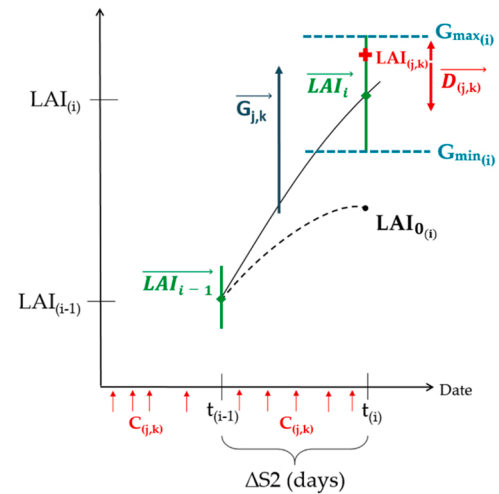


Fig. 9. Simplified scheme of the calculated $\overline{D}_{(j,k)}$ difference between $LAI_{(j,k)}$ and $LAI_{(i)}$, for $\Delta S2$ days between two consecutive S2 images obtained at $t_{(i-1)}$ and $t_{(i)}$.

$$|\Delta t| = |d_D - d_R| \quad (12)$$

2.6. Influence of the time interval between two Sentinel-2 images ($\Delta S2$)

Longer time periods between two consecutive S2 images will likely lead to longer time periods between an irrigation event and the next S2 image, also likely increasing the difficulty of the inverse problem. To test the robustness of the method, the assumed $\Delta S2$ interval of days between two consecutive S2 images is either 5, 10, and 15 days and synthetic irrigations will be injected between $t_{(i-1)} - n$ and $t_{(i)}$, with $n = 10$ days.

In order to overcome the negative effects of too long time periods between S2 images, it is possible to use interpolated LAI_{S2} values when $\Delta S2$ is higher than 5 days ($\Delta S2 = 10$ and 15, respectively). These interpolated LAI values were calculated for each day, then LAI values were recorded on a five-day window length. Those LAI values were considered as S2 measured values in our methodology likewise cloud-free S2 images were available every 5 days. Therefore, our inversion approach was tested for five cases:

1. Case I. $\Delta S2 = 5$ days

2. Case II. $\Delta S2 = 10$ days
3. Case III. $\Delta S2 = 15$ days
4. Case IV. $\Delta S2 = 5 \text{mod}_{10}$ days where the synthetic window length is fixed to 10 days then LAI values were interpolated in order to record LAI values on a 5 days basis
5. Case V. $\Delta S2 = 5 \text{mod}_{15}$ days where the synthetic window length is fixed to 15 days then LAI values were interpolated in order to record LAI values on a 5 days basis

After testing our methodology with synthetic LAI data and simulated reference irrigation dates (synthetic experiments), results are validated using real LAI measured S2 values and real irrigation dates (d_{Re}). The results are evaluated by means of detected or not-detected irrigation events and $|\Delta t|$.

3. Results

3.1. Irrigation detection accuracy metrics

This section aims at evaluating the irrigation detection approach previously described, through its ability to retrieve past irrigation dates and amounts. Three metrics are computed, relying on the notions of true positive, false positive and false negative, defined as follows. Any "probably detected irrigation" $C_{(j,k)}$ is classified as a true positive (TP) if it is detected within five days with respect to a reference irrigation date (d_R) for synthetic cases or to a real irrigation date (d_{Re}) for in situ applications. By contrast, any "probably detected irrigation" $C_{(j,k)}$ too far from these dates is classified as false positive (FP). In complement, if an irrigation is not detected, it is considered as false negative (FN).

The "Recall" (Re) is the first metric known as the overall accuracy which is related to the sensitivity of the approach for detecting irrigation dates (Eq. (13)). It is calculated as the ratio between TP and the sum of $TP + FN$ (all existing irrigation events). Therefore, a low number of FN (undetected events) favors a high value of Re. The "Precision" (Pn) is the second metric, defined as the ratio between TP and $TP + FP$ (counting all the detected events, Eq. (14)). Thus, events wrongly detected as irrigations tend to increase the value of Pn. The third metric calculates the harmonic mean between the first two metrics, yielding the so-called *F-score* (Eq. (15)) that allows the comparison of the harmonic mean of the recall and precision of the irrigation dates detection over the several cases tested.

$$Re = \frac{TP}{TP + FN} \quad (13)$$

$$Pn = \frac{TP}{TP + FP} \quad (14)$$

$$F\text{-score} = \frac{2 \times Re \times Pn}{Re + Pn} \quad (15)$$

We first discussed the detection of irrigation dates and now, "if I have the correct date, can I find the probable amount of irrigation applied?". Therefore, after retrieving the probable dates of irrigation (d_D), further investigations are performed in order to assess the irrigation amount applied. The detected dates for which the irrigation amounts are correctly retrieved are classified as d_{DA} . The percentage (P_{DA}) of all the d_{DA} (D_{DA}) over all the detected irrigation dates d_D (D_D) is calculated to assess the performance of the method in also detecting the correct amounts (Eq. (16)):

$$P_{DA} = \frac{D_{DA}}{D_D} \times 100 \quad (16)$$

3.2. Synthetic experiments

Our methodology aimed at the integration of S2-derived LAI values in Optirrig in order to detect probable previous irrigation dates and

amounts at plot scale, between two consecutive S2 images, based on an inversion approach. The irrigation retrieval approach is first tested using synthetic noisy LAI values ($LAI_{(i)}$) (Section 2.5.2). The approach is evaluated over different time periods $\Delta S2$ between two S2 images with or without resorting to interpolated LAI_{S2} values between consecutive images (Section 2.6). The accuracy metrics of Section 3.1 are used for performance evaluation.

3.2.1. Detection of irrigation dates and amounts

The method proposed for the detection of irrigation events relies on the evolution of the $\overrightarrow{D_{(j,k)}}$ vector between successive days, with a focal point on the median value of this vector. From Eq. (11), $\overrightarrow{D_{(j,k)}}$ represents the range of differences between "the range of LAI values that could have been obtained, at the S2 acquisition date $t_{(i)}$, as a result of an irrigation taking place at a previous date (j) with a given amount (k)" (a vector) and "the observed LAI value" (a scalar). The position of the median value of $\overrightarrow{D_{(j,k)}}$ vs. 0 is what catches the eye on the figures and serves as a key indication in the analysis.

As a first example, Fig. 10a, b and c show the ranges of values of $\overrightarrow{D_{(j,k)}}$ at the S2 acquisition date of 14/07 (the rightmost date on the X-axis) as a result of irrigation amounts of 20 mm (Fig. 10a), 30 mm (Fig. 9b) or 40 mm (Fig. 10c), seeking irrigation dates backwards (i.e., leftwards on the X-axis) from the S2 acquisition date at which the situation is examined. This search is extended up to the previous observation date minus ten days, as previous mentioned. A closer look at Fig. 10a, for example, indicates that an irrigation of 20 mm taking place the 07/07 would have resulted in a median $\overrightarrow{D_{(j,k)}}$ value of about $0.15 \text{ m}^2 \cdot \text{m}^{-2}$ when examining the situation, the 14/07: this means that this irrigation would have yielded a LAI value larger than the observed LAI value, the (positive) difference being $0.15 \text{ m}^2 \cdot \text{m}^{-2}$. Conversely, and irrigation of 20 mm taking place the 12/07 would have resulted in a median $\overrightarrow{D_{(j,k)}}$ value of about $-0.15 \text{ m}^2 \cdot \text{m}^{-2}$, so the predicted LAI value would have been smaller than the observed LAI value. One understands that the "detected" irrigation should have taken place between the 07/07 and 12/07, most likely at the date for which the median $\overrightarrow{D_{(j,k)}}$ value crosses the zero line (here, the 10/07 or maybe the 11/07, as indicated by the blue arrow in Fig. 10a). The same reasoning holds for Fig. 10b (irrigation amounts of 30 mm) and Fig. 10c (irrigation amounts of 40 mm) with the same detection of the irrigation date. In summary, Fig. 10a, b and c allow detecting the irrigation date but not the irrigation amount, and the detection criterion for the irrigation date is when the median $\overrightarrow{D_{(j,k)}}$ value varies from positive to negative values (C1 criterion), crossing the central zero line on the plots and by that transitioning from zero to negative values (C2 criterion).

As a second example, Fig. 10d, e and f show the ranges of values of $\overrightarrow{D_{(j,k)}}$ at the S2 acquisition date of 19/07. In Fig. 10d, moving backwards on the X-axis leads to the identification of atypical $\overrightarrow{D_{(j,k)}}$ values for the 12/07. An irrigation of 20 mm taking place the 12/07 yields a slightly negative value for the median of $\overrightarrow{D_{(j,k)}}$ whereas irrigations taking place after or before the 12/07 do not induce such an effect (red dashed circles). Fig. 10e and f also point out the effect of an irrigation taking place the 12/07, either with an amount of 30 mm (Fig. 9d) or 40 mm (Fig. 10e). The median of $\overrightarrow{D_{(j,k)}}$ is closer to zero in Fig. 10e than in Fig. 10d or e, which tends to indicate the detection of both the irrigation date (12/07) and amount (30 mm) in this case. In addition, a quasi-similar behavior of the variation on $\overrightarrow{D_{(j,k)}}$ is observed for the irrigation injected at 05/07 which could be eventually considered as a retrieved irrigation date along with 12/07. However, 05/07 was identified as a probable irrigation date when testing our approach on the 14/07 S2 acquisition previous to the acquisition date presented in Fig. 10d, e and f (19/07). Nevertheless, the common shape of these plots may seem a bit

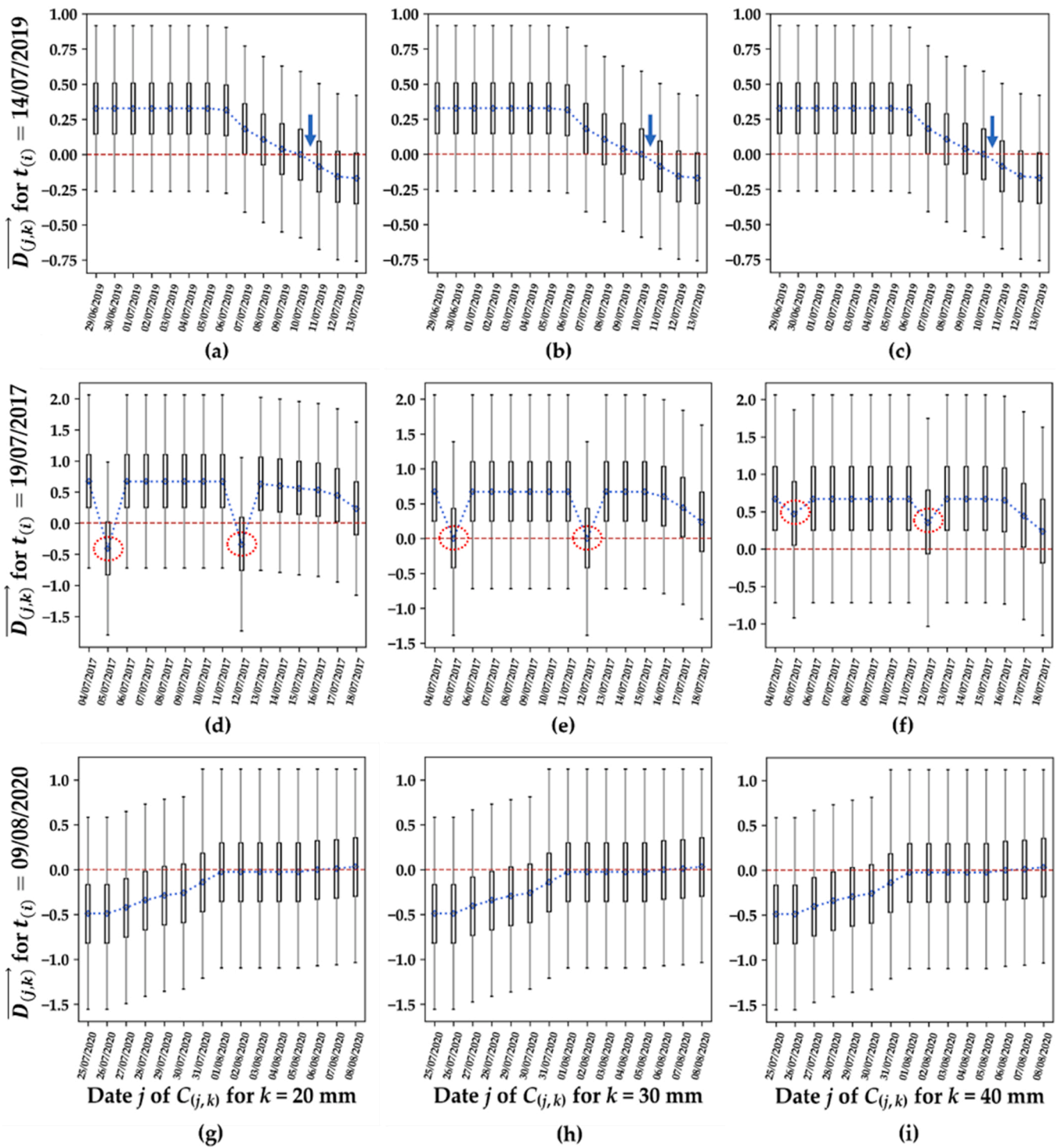


Fig. 10. The calculated $\overrightarrow{D}_{(j,k)}$ based on the difference between $LAI_{(j,k)}$ and $\overrightarrow{LAI}_{t_{(i)}}$ as a function of the date j , between $t_{(i)}$ and $t_{(i-1)} - 10$ days, of the injected irrigations $C_{(j,k)}$ represented by the non-filled boxplots in black for $k = 20, 30$ or 40 mm, respectively. In this example, the tested time lapse $\Delta S2$ between $t_{(i)}$ and $t_{(i-1)}$ is fixed to $\Delta S2 = 5$ days. The dash lines in blue represent the difference $D_{(j,k)}$ at each $t_{(i)}$ between $LAI_{(j,k)}$ and LAI_i (reference LAI at $t_{(i)}$) for $k = 20, 30$ or 40 mm, respectively. (a, b,c) Tarbes in 2019 (M2) for $t_{(i)} = 14/07/2019$; (d,e,f) Montpellier in 2017 (M1) for $t_{(i)} = 19/07/2017$; (g,h,i) Tarbes in 2020 (M3) for $t_{(i)} = 09/08/2020$.

unexpected, as it means that hypothetical irrigations occurring before or after the selected date both lead to LAI values larger than the observed value (see the discussion). The tentative criterion here is when the median $\overrightarrow{D}_{(j,k)}$ value transitions from positive to negative, moving backwards (or forwards) on the X-axis (C1 criterion).

At this stage, neither the C1 nor the C2 criteria seem able to provide a clear interpretation for the effect seemingly observed on the leftmost

part of the X-axis in Fig. 10d, e and f. This provides a third example of plots analysis and detection criteria. For an irrigation amount of 20 mm, Fig. 10d shows a transition from negative to positive values of the median of $\overrightarrow{D}_{(j,k)}$ values, whereas Fig. 10e shows the limit case of a transition from near-zero to positive values and Fig. 10f only shows positive values (overestimation of the observed LAI). This suggests a new detection criterion (C3 criterion) in the transition from negative to positive values

of the median $\overrightarrow{D_{(j,k)}}$ value.

A fourth example is provided by Fig. 10g, h and i. seeking irrigation events backwards in time from the acquisition date of 09/08. All three sketches show similar trends with only slight differences in the $\overrightarrow{D_{(j,k)}}$ values and the median of $\overrightarrow{D_{(j,k)}}$ values. Hypothetical irrigations taking place before the 01/08 would have resulted in negative median values of $\overrightarrow{D_{(j,k)}}$, thus in too low modeled LAI values, in comparison to the observed LAI value. By contrast, irrigations taking place the 01/08 or after yield to near-zero median $\overrightarrow{D_{(j,k)}}$ values, not really discriminating between dates and between amounts for the assumed uncertainties. However, given the objective to identify a given date and a given amount, and only looking at the median of $\overrightarrow{D_{(j,k)}}$ values, the detected date would be the 05/08 (or 06/08) with a 30-mm amount. The new detection criteria used here is the transition from negative to zero values of the median of $\overrightarrow{D_{(j,k)}}$ value (C4 criterion).

In a comprehensive, simplified view, the retained detection criteria are when the median $\overrightarrow{D_{(j,k)}}$ value switches from positive to negative values (C1), from zero to negative values (C2), from negative to positive values (C3) or from negative to zero values (C4). Fig. 10 was intended to illustrate the definition and use of these criteria on a limited number of typical cases, mentioning both the advantages and drawbacks. The following section evaluates the approach from a wider point of view, on all available synthetic cases.

3.2.2. Effect of $\Delta S2$ on the detection of irrigation dates and amounts

Fig. 11 summarizes the obtained accuracy metrics for the assessment of the irrigation date detection using our inversion approach, for all three experimental plots (M1, M2 and M3) and all five $\Delta S2$ cases (5, 10, 15, 5mod₁₀ and 5mod₁₅). It represents (in %) the recall (Re) (Fig. 10a), precision (Pn) (Fig. 11b) and *F-score* (Fig. 11c) at each plot and tested $\Delta S2$. A detected event (d_D) is considered an irrigation event (TP) if it is detected within an acceptable difference ($|\Delta t|$ in days) with the reference irrigation date (d_R), of 5 days which corresponds to the S2 revisit time.

For the Montpellier dataset M1, the Re-value and *F-score* reached 71.5% and 83.5%, respectively, for the $\Delta S2 = 5, 10, 5\text{mod}_{10}$ and 5mod_{15} cases but lower values (57.5% and 72.8%, respectively) for the

$\Delta S2 = 15$ case. Results show a high detection precision for M1 with a Pn reaching 100% (no false detection) over all the tested $\Delta S2$. The accuracy was slightly better for the M2 dataset of Tarbes in 2019 (M2) for the Re, Pn and *F-score* metrics, for the $\Delta S2 = 5, 5\text{mod}_{10}$ and 5mod_{15}

cases, with a 75% value for all three metrics. There was a clear decline for the $\Delta S2 = 10$ and 15 cases, down to 54% for Re, 60% for Pn and 57.5% for the *F-score*. For the M3 plot of Tarbes in 2020, 100% of the reference irrigations (d_R) were detected (Re equal to 100%) with Pn = 60% and *F-score* = 75%, respectively, for the $\Delta S2 = 5$ and 10 cases. The performances drop down to Re= 50% and *F-Score* = 66.6% for the $\Delta S2 = 15$ case. Unlike for the M1 and M2 plots, the Pn and *F-score* values increased for the M3 plot for the $\Delta S2 = 5\text{mod}_{10}$ and 5mod_{15} cases with respect to the $\Delta S2 = 10$ and 15 cases, pointing at the relevant use of interpolated LAI values.

Furthermore, $\overrightarrow{D_{(j,k)}}$ change detection analysis (described in section 3.1.1) was performed over the d_D (the detected irrigation dates) in M1 in order to retrieve the most probable amounts of water applied on each irrigation that potentially occurred. The results show that irrigation amounts information could only be retrieved over the first four d_D of the 2017 growing cycle in M1 experimental plot (between DOY 74 and 96). Five d_D over seven d_R (reference irrigations) were detected (Fig. 12a) from which four d_D showed a potential to detect the irrigation amount k . Thus, information about the potential irrigation amounts is retrieved over Montpellier with an overall accuracy of 57.1% of all the existing reference irrigation events. In addition, 80% of the detected irrigation dates (d_D) ($P_{DA} = 80\%$), showed differences over $\overrightarrow{D_{(j,k)}}$ for different injected k . In contrast, for M2 and M3, injecting $C_{(j,k)}$ of different amounts k did not show any difference over $\overrightarrow{D_{(j,k)}}$ at j , which means that it is not possible to discriminate between irrigation amounts at each detected date of irrigation and $k = 20$ mm is always considered as the most probable and sufficient irrigation amount k applied.

3.2.3. Effect of $\Delta S2$ on the performance of the detection method

Longer time periods between successive S2 images will certainly lead to less precision in the detection of irrigation dates thus to increased absolute differences ($|\Delta t|$ in days) between the date of irrigation detection (d_D) and the reference irrigation date (d_R). Fig. 12 shows $|\Delta t|$ values between zero and three, for the Montpellier plots (M1, Fig. 12a), one and two for the Tarbes plots of 2019 (M2, Fig. 12b) and 2020 (M3, Fig. 12c). However, $|\Delta t|$ is calculated only when irrigation dates have been detected. Conversely, the hatched areas in Fig. 12 indicate which irrigation dates have not been detected. This concerns the last two irrigation dates for M1 for all $\Delta S2$ cases as well as the fifth irrigation for the least favorable $\Delta S2 = 15$ case (Fig. 12a), the third irrigation date on M2 for the $\Delta S2 = 10$ and 15 cases, as well as the fourth irrigation date whatever $\Delta S2$ (Fig. 12b), the last irrigation date on M3 but only for the

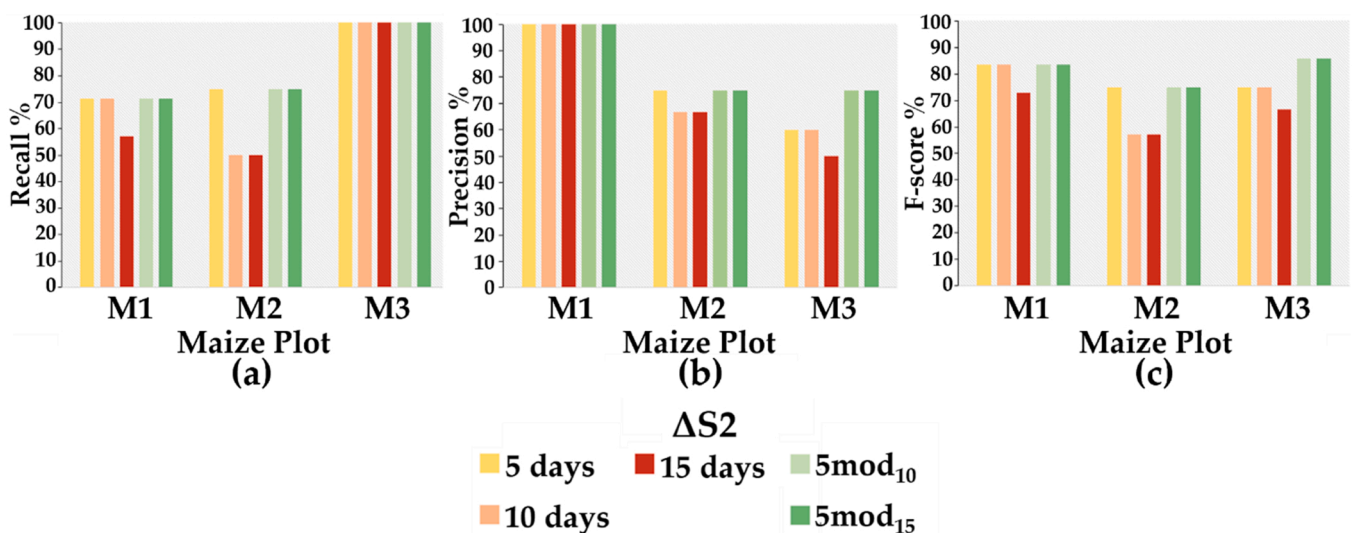


Fig. 11. The accuracy metrics of the detection of irrigation events over the maize plots of Montpellier in 2017 (M1), Tarbes in 2019 (M2) and 2020 (M3) at each of the tested spacing between two Sentinel-2 images $\Delta S2$ (5, 10, 15, 5mod₁₀ and 5mod₁₅). (a) Recall “Re”; (b) Precision “Pn”; (c) *F-score*.

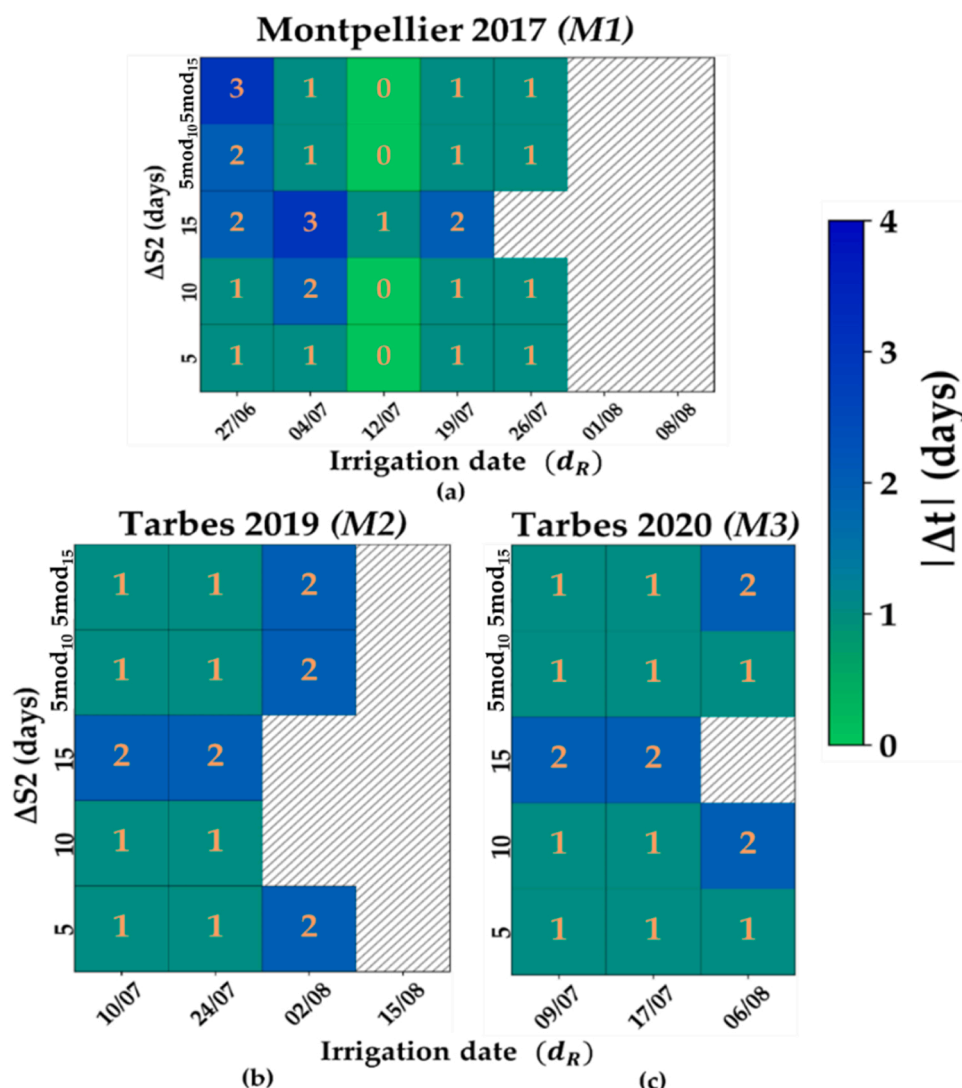


Fig. 12. The time lapse between the date of irrigation detection (d_D) and the date of the reference irrigation (d_R) ($|\Delta t| = |d_D - d_R|$) at each d_R for different tested $\Delta S2$ in days (5, 10, 15, 5mod₁₀ and 5mod₁₅). (a) Montpellier in 2017 (M1); (b) Tarbes in 2019 (M2); (c) Tarbes in 2020 (M3). The hatched area in the matrix corresponds to d_R and $\Delta S2$ cases where no irrigation is detected.

worse $\Delta S2 = 15$ case (Fig. 12c). Overall, it was expected that a method based on LAI differences in cases with or without water stress would be less relevant late in the cropping season, once the maximal LAI values are reached and when water stresses have less pronounced effects on LAI values.

In terms of $|\Delta t|$ differences, Fig. 12 a (plot M1) shows that the use of interpolated LAI values for the $\Delta S2 = 5\text{mod}_{10}$ and 5mod_{15} cases does not (always) yield significant improvements, when compared to the $\Delta S2 = 10$ and 15 cases. Although deemed useful to remedy the lack of observations over too long periods, it is expected that the hypothesis of a linear variation of LAI with time may prove wrong in certain cases: in Optirrig as in many crop models, LAI is a sigmoid function of growing degrees-days hence with no particular reason to exhibit a linear variation with time, counting time in days. This may nevertheless be true over many time intervals, making the use of LAI interpolations very performing, as can be seen on Fig. 11 a (e.g., similar $|\Delta t|$ differences for the $\Delta S2 = 5, 5\text{mod}_{10}$ and 5mod_{15} cases for the last four detected irrigations).

Fig. 12b (plot M2) and Fig. 12c (plot M3) are very similar, and pretty different from Fig. 12a. The first two irrigations are equally-well detected in all $\Delta S2$ cases ($|\Delta t|=1$ day) but with the $\Delta S2 = 5\text{mod}_{15}$ case ($|\Delta t|=2$ days). Later in the cropping season, the third irrigation in

plot M2 is only detected in the $\Delta S2 = 5, 5\text{mod}_{10}$ and 5mod_{15} cases ($|\Delta t|=2$) which promotes the use of interpolated LAI values as a surrogate to missing LAI observations. The fourth irrigation in plot M3 is detected in the $\Delta S2 = 5, 10, 5\text{mod}_{10}$ and 5mod_{15} cases, discarding thus the least favorable $\Delta S2 = 15$ case and offering similar (good) performances in the $\Delta S2 = 5$ and 5mod_{10} cases ($|\Delta t|=1$ day) on the one hand, and in the $\Delta S2 = 10$ and 5mod_{15} cases ($|\Delta t|=2$ days) on the other hand, somehow regaining temporal information from the use of interpolated LAI values.

3.3. Detection of irrigation events using real Sentinel-2 values

The poor availability of cloud-free S2 images could hamper the detection of irrigation events and prove problematic for plot supervision purposes and for the management of irrigated territories, especially in critical water requirement stages (pollination and kernel development, (García y García et al., 2009)). The previous sections, leaning on synthetic experiments, revealed a promising potential of the interpolated noisy LAI values (referred to as the $\Delta S2 = 5\text{mod}_{10}$ and 5mod_{15} cases) for irrigation detection. The inversion method is tested here against real data, relying on LAI_{S2} observations and associated interpolated values (LAI_{int}) to explore a modified $\Delta S2 = 5\text{mod}$ case in which LAI values used each 5 days arise either from observed or from interpolated LAI values

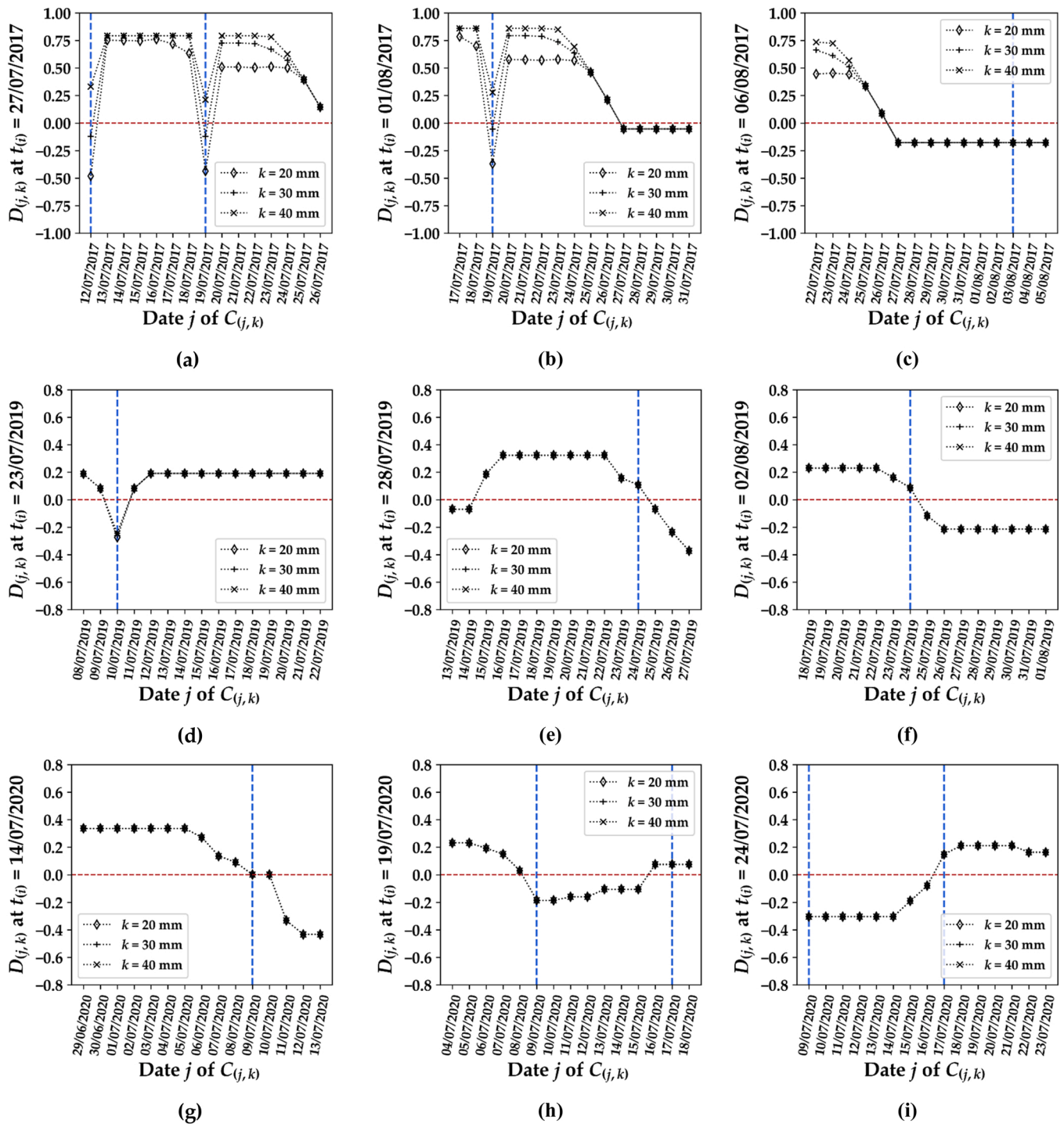


Fig. 13. The calculated $D_{(j,k)}$ based on the difference between $LAI_{(j,k)}$ and LAI_{int} as a function of the date j , between $t_{(i)}$ and $t_{(i-1)} - 10$ days, of the injected irrigation $C_{(j,k)}$ represented by the black lines for.

(Fig. 13, designed as Fig. 10). From the previous sections, the detection criteria are when the median $\overrightarrow{D_{(j,k)}}$ value switches from positive to negative values (C1 criterion), from zero to negative values (C2 criterion), from negative to positive values (C3 criterion) or from negative to zero values (C4 criterion).

$k = 20, 30$ and 40 mm. The dash lines in blue represents the real irrigation dates (d_{Re}). (a,b,c) Montpellier in 2017 (M1) for $t_{(i)} = 27/07/2017, 01/08/2017$ and $06/08/2017$; (d,e,f) Tarbes in 2019 (M2) for $t_{(i)} = 23/07/2019, 28/07/2019$ and $02/08/2019$; (g,h,i) Tarbes in 2020 (M3) for $t_{(i)} = 14/07/2020, 19/07/2020$ and $24/07/2020$.

The detection approach was tested for the three experimental plots of Montpellier in 2017 (M1 plot, Fig. 13a, b and c) and Tarbes in 2019 (M2 plot, Fig. 13d, e and f) and 2020 (M3 plot, Fig. 13h, i and j). In these plots the real irrigations dates (d_{Re}) are represented by the blue dashed lines. In Fig. 13 a, the detection criteria C3 ($j = 12/07/2017$) then C1 and C3 ($j = 19/07/2017$) are met and the most likely irrigation amount is 30 mm in both cases, judging from the median values of $\overrightarrow{D_{(j,k)}}$. In Fig. 13b, the same irrigation date ($j = 19/07/2017$) is detected by the irrigation criteria C1 and C3. By contrast, none of the criteria is able to detect the irrigation taking place at $j = 06/08/2017$ in Fig. 13c –

probably because this date comes late in the cropping season, with expected plateau values of the LAI (and possibly less pronounced effects of missed irrigations than during the quick growth period). In Fig. 13d and e, the detected irrigation dates are 10/07/2019 from the C1 and C3 criteria, and 25/07/2019 from the C1 criterion, missing the target by one day in the latter case. In Fig. 13f, the C3 criterion allows a corrected detection of the irrigation date (24/07/2019 previously seen as 25/07/2019). This emphasizes the interest of overlaps between sliding, temporal windows when applying the detection method over a complete irrigation season. Unlike Fig. 13a, b and c, Figs. 13d, e and f exhibits no differences between irrigation amounts thus not allowing any detection of the irrigation amount (at least between the tested 20, 30 and 40-mm values).

Fig. 13g offers a case in which the interpretation may hesitate between the detection of the (correct) irrigation date (09/07/2020) from the C2 criterion, or the slightly wrong detection of another date (11/07/2020) from the C1 criterion. This hesitation prompts to consider the C2 criterion not only as a "partial" C1 criterion (that would denote an incomplete effect) but also as an "early warning" to question the C1 criterion, typically when the detection curve shows a plateau value. By analogy, the same remark should apply for the C4 criterion with respect to the C3 criterion. The C1 criterion performs quite well in Fig. 13h to identify the real irrigation date (09/07/2020) although with an ambiguity with the 08/07/2020, as the median of $\overrightarrow{D_{(j,k)}}$ crosses the zero-line between these two days (this ambiguity seems inherent to the definition of the C1 and C2 criteria). Also, in Fig. 13h, the irrigation detection for the 15/07/2020 or the 16/07/2020 may be corrected when looking at the information displayed in Fig. 13i, allowing to identify the real date (17/07/2020).

Fig. 13 also illustrates a few cases of false detections when applying the C1 or C2 criteria (Fig. 13b, 26/07/2017 or 27/07/2017), the C2 criterion (Fig. 13c, 27/07/2017, unfortunately in correlation with the preceding case) or the C4 criterion (Fig. 13e, 14/07/2019). In a wider view, the topic of detection accuracy is tackled by calculating the Recall "Re", Precision "Pr" and F-score metrics (Fig. 14). This inversion approach (used alone, in autonomous manner, i.e., not resorting to any complementary information arising from radar data for soil surface moisture or from known field practices in terms of irrigation scheduling or triggers) was able to detect 70% (plot M1), 75% (plot M2) and 100% (plot M3) of the irrigation events (Re values). This was done with good precision, from the Pn values (77% for M1, 75% for M2 and M3) that signal a limited number of false detections. The associated F-score values (73% for M1, 75% for M2 and 85% for M3) range from "pretty good" to

"good" (F-score above 80%) which denotes the potential of this inversion method, used alone or in combination with other so-called inversion constraints for of operational purposes (see the discussion section).

From the previous sections, the outcome of the analysis is the selection of the irrigation dates (d_D) for which the median of the noisy differences between predictions and observations, at the dates of available observations, is (i) as close as possible to zero and (ii) fulfills at least one of the selected criteria related to its evolution in time. These criteria belong to the "change detection" type of approach often used when working on signal analysis and remote sensing products. For the details of the inversion process and these of the selection criteria to identify the irrigation events, see Figs. 10 and 13 and the associated comments.

For operational purposes, the indication of irrigation dates should be complemented by that of irrigation amounts. We thus compared the detected amounts (I_D) with the real amounts (I_R) on the M1, M2 and M3 plots, while using interpolated LAI_{S2} values to obtain an apparent, regular time period of 5 days between successive images. Fig. 15 shows both the detected dates and irrigation amounts, in comparison with the real field data, displaying all observed Sentinel-2 LAI values and positioning them within the vegetative or reproductive stages, also indicating the missed irrigation detection, the false detections and the correct detections, with the associated absolute time difference ($|\Delta t|$ in days) between the detected and the real irrigation dates. In Fig. 15, light grey and dark grey bars correspond to the real and the detected amount of irrigation, respectively. Thus, a true irrigation date detection occurred when a dark grey bar is represented along with a light grey bar at each real irrigation date. Additionally, a false irrigation detection (false positive) would be observed, in Fig. 15, as a single dark grey bar meaning that our approach has detected an irrigation that does not refer to a real irrigation date. Conversely, an undetected irrigation date (false negative) would be observed as a single light grey bar, meaning that our approach failed to detect an irrigation date.

Strikingly, Fig. 15a shows $|\Delta t| = 1$ -day values in the vegetative stage, degraded into $|\Delta t| = 2-3$ days values during the reproductive stage, in which 3 missed detections occurred, late in the cropping season, in the senescence phase and less than 30 days before harvest. In the present work, Fig. 15 shows only four false positive date detections (Fig. 15a: DOY=169 and 218, Fig. 15b: DOY=196, Fig. 15c: DOY=208). In addition, four events have been undetected, the last three in Fig. 15a (DOY=248, 256, 259) and the last one in Fig. 15b (DOY=227). This illustrates one of the expected limits of this approach that relies on the ascending dynamics of the LAI variable. This limit may also explain the presence of false detections in the reproductive stage (one example in Fig. 15a).

Overall, the same trends to larger $|\Delta t|$ values in the reproductive stages are visible in Fig. 15b and c, together with increased difficulties in detecting the irrigations as the harvest date approaches. By contrast, even if the method performs well in most cases, the issue of false detections seems more difficult to handle. To deal with it in appropriate manner, it may prove useful to identify a catalog of problematic or limit cases.

In order to detect valuable information about the applied amounts of irrigation water, further investigation was performed on $\overrightarrow{D_{(j,k)}}$ change detection analysis over the d_D (the detected irrigation dates) in M1. A dose of $k = 30$ mm was detected as the most probable amount of irrigation over two d_D (12/07/2017 and 19/07/2017) of seven detected irrigation dates d_D among the 10 real irrigation dates d_{Re} .

Therefore, for Montpellier (M1), only over two detected irrigations (d_D) we were able to retrieve information about the applied irrigation amount among ten real irrigation dates (d_{Re}) from which seven dates were detected (d_D). Thus, information about the potential irrigation amounts is retrieved over Montpellier with a relatively low overall accuracy of 20% of all the existing real irrigation events (d_{Re}) and a P_{DA} of 28.5% (amounts were retrieved for two d_D over seven d_D). In contrast,

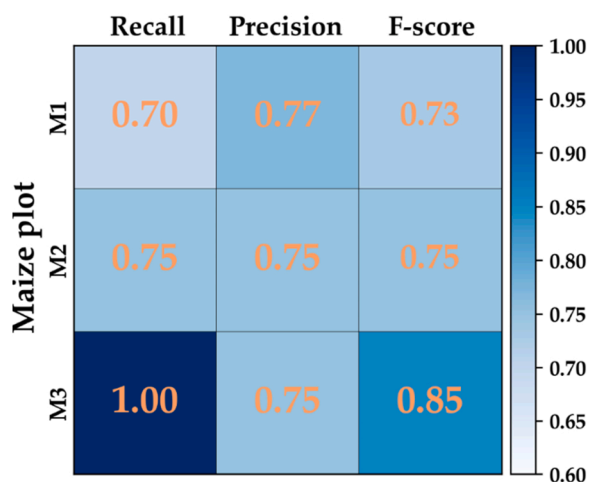


Fig. 14. The accuracy metrics (Recall, Precision and F-score) of the detection of irrigation events over the maize plots of Montpellier in 2017 (M1), Tarbes in 2019 and 2020, M2 and M3, respectively.

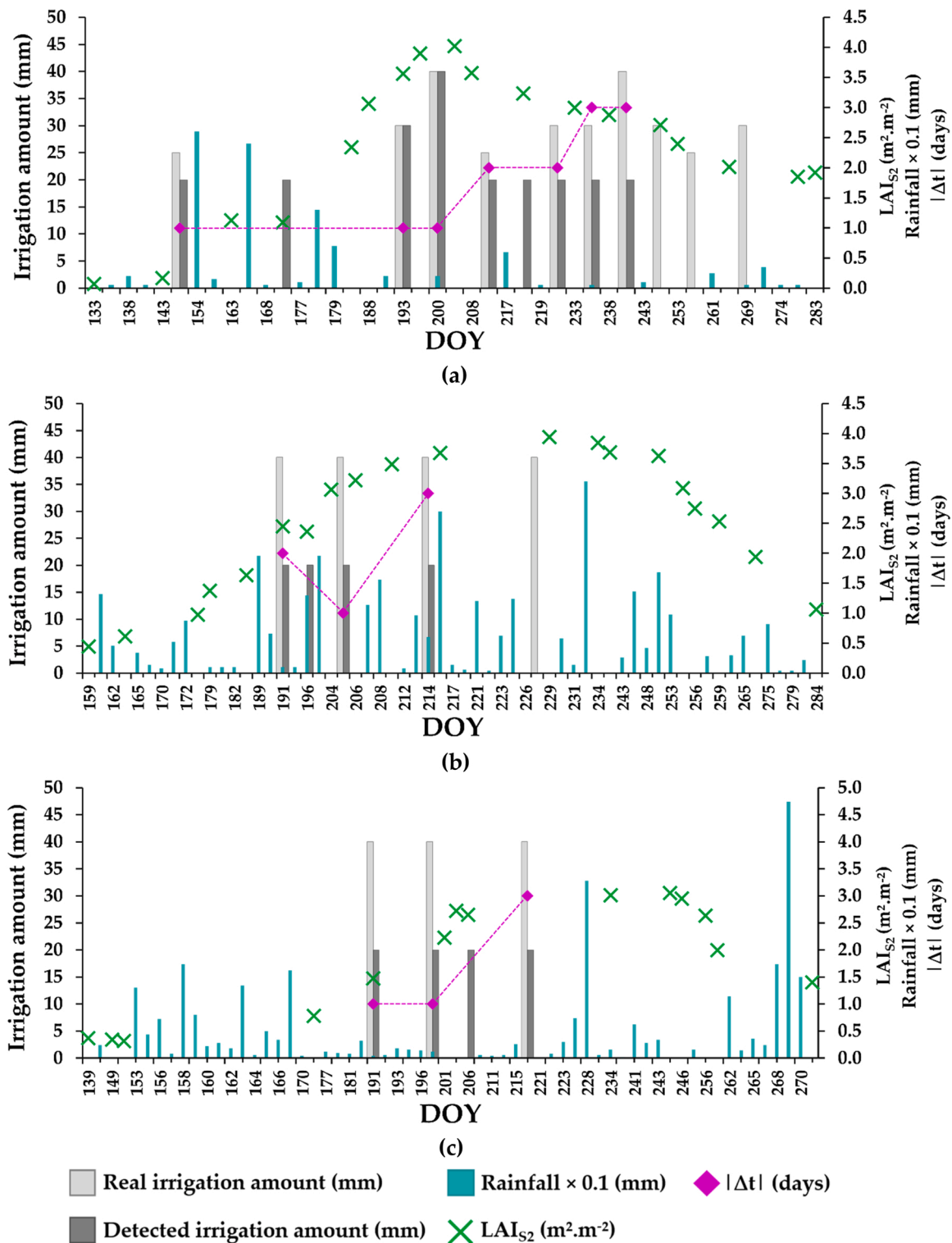


Fig. 15. Real irrigation amounts (light grey bars), detected irrigation amounts (dark grey bars) applied at each real date of irrigation (d_{Re}), S2 derived LAI values (LAI_{S2}), daily precipitation data and the time lapse between the date of irrigation detection (d_D) and the date of the real irrigation (d_{Re}) ($|\Delta t| = |d_D - d_{Re}|$) at each d_{Re} (real irrigation dates, grey bars) over the maize growing season. (a) Montpellier in 2017 (M1); (b) Tarbes in 2019 (M2); (c) Tarbes in 2020 (M3).

for M2 and M3, $\overrightarrow{D_{(j,k)}}$ investigation was unable to discriminate between irrigation amounts at each detected date of irrigation. Thus, $k = 20$ mm is always considered as the most probable irrigation amount k applied, at d_D , because no differentiation was observed when injecting irrigations with different amounts ($k = 20, 30$ and 40 mm).

4. Discussion

4.1. Position of this work within other irrigation detection works

The detection of irrigation dates and amounts is a challenge which would allow easiest supervision of irrigated territories, providing insights on the real, in-situ practices in resources management and partial,

complete or excessive fulfilment of crop water demands. Detecting irrigation events with remote sensing requires handling the complexity and variations of maize spectral responses to irrigation on the one hand, and water stress on the other hand (Chen et al., 2018). So far, studies have shown that water stress at various stages in maize leads to significant decreases in the leaf area index (Myers et al., 2017; Zhou et al., 2020) and the photosynthetic capacity (Chaves et al., 2009; Efeoğlu et al., 2009) with significant effects on maize spectral reflectance characteristics (Feng et al., 2013) finally used to detect irrigation and stress events.

From a completely different perspective, this research used a novel approach for irrigation detection through the integration of Sentinel-2 derived LAI (LAI_{S2}) in the Optirrig model, solving the inverse problem of identifying the irrigation events able to explain the observed LAI_{S2} values. In this approach, the sine qua non condition to be able to detect an irrigation (date, amount) is thus that irrigation has the targeted effect on the LAI dynamics simulated by Optirrig, i.e., the effect of taking the simulated LAI value close enough to the LAI_{S2} value. However, a first difficulty arises from the uncertainty (or equifinality) in the amount of water needed for a given crop development between two LAI_{S2} observations: different water amounts (rain or irrigation, or rain and irrigation) may lead identical crop growth (and different drainage values). A second difficulty stems from the time lag between the irrigation and the associated LAI response, which also hamper the detection of irrigation events (Gumma et al., 2011; Velpuri et al., 2009), in both cases due to the apparent or partial decorrelation between the cause and the effect. Thus, the critical step in detecting irrigation information is to successfully establish the relationship between the chronicle of observed LAI_{S2} values on one side, crop growth and water needs simulated by Optirrig on the other side. Therefore, for a probable irrigation date, we aim at evaluating the effect of different cases of water amounts applied in which the simulated LAI is sensitive to the irrigation amount, and cases in which it is not but there is information in each case, (i) if an irrigation amount larger than the reference amount causes an increase in the simulated LAI value, then the reference irrigation amount was responsible for some water stress, (ii) if an irrigation amount larger than the reference amount does not cause any increase in the simulated LAI value, then the reference irrigation amount was either just enough to avoid water stress, or already excessive, (iii) if an irrigation amount smaller than the reference amount does not cause any decrease in the simulated LAI value, then the reference amount was already excessive, (iv) if an irrigation amount smaller than the reference amount causes a decrease in the simulated LAI value, then the reference amount was either just enough to avoid water stress or already responsible for some water stress. In other words, testing a wide enough set of irrigation amounts (between 0 and the maximal plausible amount) allows covering all cases.

The combined use of LAI_{S2} and Optirrig crop model has shown a great potential in the monitoring of agricultural water use and irrigation detection. In fact, several studies have noted that the approach combining optical remote sensing products, such as the Normalized Difference Vegetation Index (NDVI) and LAI, and crop models have become necessary for more accuracy in vegetation monitoring (Huang et al., 2019; Saadi et al., 2015; Zwart et al., 2010). Such couplings also tend to become popular for water resources and irrigation water supplies monitoring at the plot and regional scales (Abi Saab et al., 2021; Beyene et al., 2022; Zhang et al., 2019).

In the present work, the irrigation events (triggered by the estimated crop water needs, and decided from one of the several ways to generate irrigation strategies) and the LAI dynamics were both simulated by Optirrig for the experimental plots. Meanwhile, the observation data were affected by errors of the Gaussian noise type, within realistic ranges drawn from literature. Then the robustness of the inversion method was first assessed for five so-called synthetic cases of "temporal spacing" between LAI_{S2} observations, noted $\Delta S2 = 5, 10, 15, 5\text{mod}_{10}$ and 5mod_{15} , where 5, 10 and 15 indicate a number of days between

observations while 5mod_{10} and 5mod_{15} indicate that interpolated, fictitious LAI values have been used to fill the gap and feed the inversion process. As expected, the $\Delta S2 = 5$ case yielded the best results, closely followed by the $\Delta S2 = 5\text{mod}_{10}$ and 5mod_{15} cases, allegedly working well as a surrogate to the lack of enough cloud-free images, both for the synthetic and real, in situ applications. The Recall, Precision and F-score accuracy metrics attest the relevance of the method for the favorable $\Delta S2$ cases.

4.2. Performances, limitations, improvements and complements for operational purposes

The results of the synthetic experiments (illustrated in Section 3.2) demonstrate that the poor availability of cloud-free S2 observations could be a reason for the degradation of the irrigation dates retrieval performance. A bit more into details, the degradation of results quality observed with the least favorable $\Delta S2$ cases comes in line with previous works (e.g., Battude et al., 2017) which highlighted the high importance of the satellite revisit time, with several detrimental effects of too long revisit times. The most complicated situation is when the three following conditions occur altogether, (i) large time periods exist between successive Sentinel-2 images, (ii) the soil-crop system has to recover from water stress conditions, it has been irrigated but only weakly responds (and with inertia) to this irrigation in terms of transpiration and associated LAI growth (Duchemin et al., 2006) as a consequence of physiological processes, and (iii) the mentioned irrigation comes either too close (not visible yet) or too far (not visible anymore) from the most recent Sentinel-2 image. Although sometimes experimenting these situations in the present work, most irrigation dates could be detected with an absolute difference of 0, 1 or 2 days between the reference and the detected irrigation date – which seems enough for most practical purposes.

General insights may be drawn from the results of the approach when testing the irrigation detection methodology using real LAI S2 observations' values. It seems very likely that the correct detection of irrigation amounts will be hampered by the fact that the farmers do not follow spontaneously the irrigation decisions that would advise by Optirrig, in terms of irrigation triggers, criteria and doses. In fact, the maize crop is characterized by high and critical water requirements meaning that it is more susceptible to water deficit and stress, especially during the period that falls between the vegetative and the beginning of the reproductive growth stages (Piscitelli et al., 2022). This explains the significant effect of applying different amounts of irrigation on the crop development and LAI. Moreover, there are multiple possibilities of thinking the irrigation strategies in Optirrig, depending on the assigned objectives and the contextual constraints. Conversely, prior knowledge on the contextual constraints (e.g., water turn, limited resources availability or restriction of use) and decision rules of the farmers would help pre-selecting the correct parameterization of irrigation strategies in Optirrig, i.e., the parameters rightfully adjusted during the inversion process. This should be regarded as one of the several ways to usefully constrain the inversion process. Here, irrigations were decided by Optirrig as soon as the filling of the available water reserve dropped under about 70% (Table 3) and the applied dose was selected among the 20, 30 or 40 mm amounts, so as to fill again the available water reserve (the needed amount depends on the extension of the root zone on the day the decision is made).

Three false positive date detections were noted, two of which during the early stages of maize growth, where irrigation is most needed for crop growth in absence of rain but rain could obviously be mistaken for irrigation, in the circumstances previously described in the discussion. In addition, the non-detection of irrigation dates (false negative) is due to the difficulties in applying the inversion approach for stable or slowly decreasing LAI values late in the cropping season but also to the chosen parameterization for the irrigation strategies, see Table 3 and the Management parameters: the indicated sowing dates (DOY=105 for the

M1 plot, DOY=121 for the M2 and M3 plots) combined with the indicated "temporal windows" for irrigation (140 days for M1, 115 days for M2 and M3) simply prevented the model from detecting any irrigation taking place after DOY= 245 on the M1 plot (Fig. 15a) and DOY= 236 on the M2 plot (Fig. 15b). This questionable parameterization was chosen on purpose to illustrate the vulnerability of the method when insufficiently related to field practices (and also because it neither affected the methodology nor the evaluation proposed).

On the other hand, the sensitivity of the crop development (LAI) to irrigation and water availability have shown to be lower in late stages of the maize growing season (after the flowering stage) which has mainly led to false negative irrigation detections. In fact, several studies found that LAI is sensitive to irrigation during early stages of crop development, but its response to irrigation can vary depending on the species, growing conditions, and stage of crop development (Farooq et al., 2011; Huang et al., 2022; Si et al., 2020). For instance, a study by Huang et al. (2022) found that summer maize LAI was more sensitive to irrigation during the early stages of crop development compared to later reproductive stages. In coherence, the sensitivity of the LAI, simulated through crop modeling, to soil water availability and dynamics have shown to be lower in reproductive growing stages compared to the vegetative stages of crop development (Silvestro et al., 2017; Varella et al., 2012) which has high negative influence of the performance of the irrigation detection approach.

Similarly, it seems difficult anyway to detect any late irrigation that would be unneeded from the water balance perspective of Optirrig but still applied by the farmers for grain filling purposes (or to prevent soil crusting, le Page et al., 2014).

More generally, the precision in the detection of irrigation dates, through crop modelling, is closely linked to the accuracy of weather, soil and field data, as uncertainties on these factors always impact the performance of crop models (Huang et al., 2019; Li et al., 2015). Thus, the extensive and complementary use of several sources of external and independent data, such as radar and optical data, is considered of great interest in several irrigation mapping or detection and other crop monitoring approaches (Ozdogan et al., 2010; Ndikumana et al., 2018; Bazzi et al., 2021) in order to inform the crop models and in turn reduce their uncertainties. In the present case, it would likely be very beneficial to feed the inversion process with both soil surface moisture estimates (radar data) and LAI observations (optical data), so as to constrain both the water balance and the crop growth schemes of Optirrig.

Promising radar-only approaches have already been promoted in the recent literature. Le Page et al. (2020) proposed a methodology to detect irrigation timing using time series of surface soil moisture derived from Sentinel-1 radar observations and a water balance model. The method provided satisfactory results and accuracy in retrieving the timing of the irrigation events with an F-score that ranges between 80% and 83%. Bazzi et al. (2020) used a change detection model for detecting irrigation episodes at plot scale using Sentinel-1 synthetic aperture radar data. The results showed that 74.1% of the irrigation events could be detected with a *F-score* of 76.4%, also pointing out the interest of using additional information relative to irrigation (irrigation method, range of possible irrigation amounts) and crop phenology (expected crop water needs and ranges of evapotranspiration rate) to constrain the inversion process. An important question could be addressed concerning the irrigation method used which highly affects soil moisture levels and by that soil surface moisture estimates and the performance of the irrigation detection approach (Ouaadi et al., 2021).

5. Conclusions

The present work aimed at the detection of irrigation dates and amounts on maize plots, as the result of an inversion process seeking the coincidence between (observed) Sentinel-2 derived Leaf Area Index values and (estimated) LAI values provided by the Optirrig crop model. The accuracy and robustness of the method were first tested against a

wide variety of synthetic but realistic cases, all built as plausible variants of the real, documented situations found in three experimental plots located in the Occitanie Region, in the south of France (near Montpellier and Tarbes). The method was then applied as for operational purposes (e.g., supervision of irrigated territories) so as to identify its abilities, merits and drawbacks, as well as ways of improvements.

Three metrics (Recall, Precision, F-score) were used to assess the performance of the inversion in retrieving the correct dates and amounts in more or less degraded situations, depending on the $\Delta S2$ time period between two successive cloud-free Sentinel-2 images, leaning on the number of false negative (undetected), false positive (wrongly detected) and true positive detections. The tested cases for $\Delta S2$ values were 5, 10, 15, 5mod₁₀ and 5mod₁₅ days, the latter two notations indicating the use of interpolated LAI values as a surrogate to the missing values, forming artificial $\Delta S2 = 5$ days cases. On the synthetic dataset of irrigation events, the best detection performances were obtained from the $\Delta S2 = 5, 5\text{mod}_{10}$ and 5mod_{15} cases with a F-score of 84.3%. In addition, the absolute $|\Delta t|$ difference between the detected and the reference irrigation dates was 0, 1 or 2 days in a large majority of cases, and never exceeding 3 days. The detection of irrigation amounts was less efficient for the synthetic dataset associated with the humid climate of Tarbes than for that associated with the (nearly) semi-arid climate of Montpellier, in which the correct irrigation amount was detected in 80% of the cases.

Then testing the inversion process against real data has shown promising results, as the Recall (ratio between the true positive and the sum of true positive and false negative) was 81.6% while the Precision (ratio between the true positive and the sum of true positive and false positive) was 75.6%. Meanwhile, the detailed, one-by-one analysis of the results has allowed identifying the weaknesses and cases of failure of the otherwise reliable four detection criteria derived from the synthetic experiments. However, the detection of irrigation amounts was even more difficult when handling the real data than for the synthetic data. But the answer is known: Optirrig has several ways to describe irrigation strategies and better results regarding the detection of irrigation amounts would be obtained when using the parameterization of irrigation strategies that matches the most the local irrigation practices and decision rules.

This brings in the idea of introducing external information and constraints to facilitate the inversion process, which surely is a valuable perspective for future operational applications of the method over given plots or wide irrigated territories. For example, it seems very obvious that the combined use of soil surface moisture estimates (radar data) and LAI observations (optical data) would be very beneficial to the inversion process by informing and constraining both the water balance and the crop growth schemes of Optirrig, knowledge is available to follow this lead and meet the societal expectations of more virtuous agricultural water management. Furthermore, it would be useful to think about coupling S2 data with historical Landsat data that cover multiple decades, to obtain more robust S2 time-series and enhance the performance of the irrigation detection and monitoring. In fact, Landsat data, provide sufficiently dense time series data to permit seasonal modeling, at high spatial resolution, when integrated with S2 optical time series.

Declaration of Competing Interest

The authors declare that they have no known competing financial interests or personal relationships that could have appeared to influence the work reported in this paper.

Data availability

Data will be made available on request.

Acknowledgments

This research received fundings from the French Space Study Center (CNES, TOSCA 2022 project), the National Research Institute for Agriculture, Food and the Environment (INRAE) and the RSEAU project financed by the French Environment and Energy Management Agency (ADEME). The authors also wish to thank Campus France for partially financing M. Hamze's PhD thesis, the European Space Agency (ESA) for the Sentinel-1 data, and the French Land Data Center (Theia) for providing Sentinel-2 data corrected from atmospheric effects.

References

- A, Z., Maitra, S., 2018. Crop modeling: a tool for agricultural research. *MOJ Food Process. Technol.* 6. <https://doi.org/10.15406/mojfpt.2018.06.00186>.
- Abi Saab, M.T., el Alam, R., Jomaa, I., Skaf, S., Fahed, S., Albrizio, R., Todorovic, M., 2021. Coupling remote sensing data and aquacrop model for simulation of winter wheat growth under rainfed and irrigated conditions in a mediterranean environment. *Agronomy* 11. <https://doi.org/10.3390/agronomy11112265>.
- Abuzar, M., McAllister, A., Whitfield, D., 2015. Mapping irrigated farmlands using vegetation and thermal thresholds derived from landsat and ASTER data in an irrigation district of Australia. *Photo Eng. Remote Sens.* 81. <https://doi.org/10.14358/PERS.81.3.229>.
- Allen, R.G., Pereira, L.S., Raes, D., Smith, M., a B, W., 1998. Crop evapotranspiration - Guidelines for computing crop water requirements - FAO Irrigation and drainage paper 56. *Irrig. Drain.* <https://doi.org/10.1016/j.eja.2010.12.001>.
- Ambika, A.K., Wardlow, B., Mishra, V., 2016. Remotely sensed high resolution irrigated area mapping in India for 2000 to 2015. *Sci. Data* 3. <https://doi.org/10.1038/sdata.2016.118>.
- Araus, J.L., Kefauver, S.C., Zaman-Allah, M., Olsen, M.S., Cairns, J.E., 2018. Translating high-throughput phenotyping into genetic gain field phenotyping is a bottleneck for crop genetic improvement. *Trends Plant Sci.*
- Aubert, M., Baghdadi, N., Zribi, M., Douaoui, A., Loumagne, C., Baup, F., el Hajj, M., Garrigues, S., 2011. Analysis of TerraSAR-X data sensitivity to bare soil moisture, roughness, composition and soil crust. *Remote Sens Environ.* 115. <https://doi.org/10.1016/j.rse.2011.02.021>.
- Aubert, M., Baghdadi, N.N., Zribi, M., Ose, K., el Hajj, M., Vaudour, E., Gonzalez-Sosa, E., 2013. Toward an operational bare soil moisture mapping using terrasars-x data acquired over agricultural areas. *IEEE J. Sel. Top. Appl. Earth Obs. Remote Sens.* 6. <https://doi.org/10.1109/JSTARS.2012.2220124>.
- Ban, H.Y., Ahn, J.B., Lee, B.W., 2019. Assimilating MODIS data-derived minimum input data set and water stress factors into CERES-Maize model improves regional corn yield predictions. *PLoS One* 14. <https://doi.org/10.1371/journal.pone.0211874>.
- Bastiaanssen, W.G.M., Molden, D.J., Makin, I.W., 2000. Remote sensing for irrigated agriculture: Examples from research and possible applications. *Agric. Water Manag.* 46. [https://doi.org/10.1016/S0378-3774\(00\)00080-9](https://doi.org/10.1016/S0378-3774(00)00080-9).
- Battude, M., al Bitar, A., Morin, D., Cros, J., Huc, M., Marais Sicre, C., le Dantec, V., Demarez, V., 2016. Estimating maize biomass and yield over large areas using high spatial and temporal resolution Sentinel-2 like remote sensing data. *Remote Sens Environ.* 184. <https://doi.org/10.1016/j.rse.2016.07.030>.
- Battude, M., al Bitar, A., Brut, A., Tallec, T., Huc, M., Cros, J., Weber, J.J., Lhuissier, L., Simonneau, V., Demarez, V., 2017. Modeling water needs and total irrigation depths of maize crop in the south west of France using high spatial and temporal resolution satellite imagery. *Agric. Water Manag.* 189. <https://doi.org/10.1016/j.agwat.2017.04.018>.
- Bazzi, H., Baghdadi, N., Ienco, D., Hajj, M., el Zribi, M., Belhouchette, H., Escorihuela, M.J., Demarez, V., 2019. Mapping irrigated areas using Sentinel-1 time series in Catalonia, Spain. *Remote Sens (Basel)* 11. <https://doi.org/10.3390/rs11151836>.
- Bazzi, H., Baghdadi, N., Fayad, I., Charron, F., Zribi, M., Belhouchette, H., 2020a. Irrigation events detection over intensively irrigated grassland plots using sentinel-1 data. *Remote Sens (Basel)* 12. <https://doi.org/10.3390/rs12244058>.
- Bazzi, H., Baghdadi, N., Fayad, I., Zribi, M., Belhouchette, H., Demarez, V., 2020b. Near real-time irrigation detection at plot scale using sentinel-1 data. *Remote Sens (Basel)* 12. <https://doi.org/10.3390/rs12091456>.
- Bazzi, H., Baghdadi, N., Amin, G., Fayad, I., Zribi, M., Demarez, V., Belhouchette, H., 2021. An operational framework for mapping irrigated areas at plot scale using sentinel-1 and sentinel-2 data. *Remote Sens (Basel)* 13. <https://doi.org/10.3390/rs13132584>.
- Beyene, A.N., Zeng, H., Wu, B., Zhu, L., Gebremicael, T.G., Zhang, M., Bezabih, T., 2022. Coupling remote sensing and crop growth model to estimate national wheat yield in Ethiopia. *Big Earth Data* 6. <https://doi.org/10.1080/20964471.2020.1837529>.
- Biagini, B., Bierbaum, R., Stults, M., Dobardzic, S., McNeelley, S.M., 2014. A typology of adaptation actions: A global look at climate adaptation actions financed through the Global Environment Facility. *Glob. Environ. Change* 25. <https://doi.org/10.1016/j.gloenvcha.2014.01.003>.
- Bouman, B.A., 1995. Crop modelling and remote sensing for yield prediction. *Neth. J. Agric. Sci.* 43. <https://doi.org/10.18174/njas.v43i2.573>.
- Bousbih, S., Zribi, M., Hajj, M., el, Baghdadi, N., Lili-Chabaane, Z., Gao, Q., Fanise, P., 2018. Soil moisture and irrigation mapping in a semi-arid region, based on the synergetic use of Sentinel-1 and Sentinel-2 data. *Remote Sens (Basel)* 10. <https://doi.org/10.3390/rs10121953>.
- Brisson, N., Gary, C., Justes, E., Roche, R., Mary, B., Ripoche, D., Zimmer, D., Sierra, J., Bertuzzi, P., Burger, P., Bussière, F., Cabidoche, Y.M., Cellier, P., Debaeke, P., Gaudillère, J.P., Hénault, C., Maraux, F., Seguin, B., Sinoquet, H., 2003. An overview of the crop model STICS. *Eur. J. Agron.* [https://doi.org/10.1016/S1161-0301\(02\)00110-7](https://doi.org/10.1016/S1161-0301(02)00110-7).
- Brown, J.F., Pervez, M.S., 2014. Merging remote sensing data and national agricultural statistics to model change in irrigated agriculture. *Agric. Syst.* 127. <https://doi.org/10.1016/j.agry.2014.01.004>.
- Burney, J., Woltering, L., Burke, M., Naylor, R., Pasternak, D., 2010. Solar-powered drip irrigation enhances food security in the Sudano-Sahel. *Proc. Natl. Acad. Sci. USA* 107. <https://doi.org/10.1073/pnas.0909678107>.
- Cantelaube, P., Carles, M., 2015. Le Registre Parcellaire Graphique: des données géographiques pour décrire la couverture du sol agricole. *Cah. Des. Tech. De. l'INRA* 58-64.
- Castañeda-Vera, A., Lefelaar, P.A., Álvaro-Fuentes, J., Cantero-Martínez, C., Mínguez, M.I., 2015. Selecting crop models for decision making in wheat insurance. *Eur. J. Agron.* 68. <https://doi.org/10.1016/j.eja.2015.04.008>.
- Chaves, M.M., Flexas, J., Pinheiro, C., 2009. Photosynthesis under drought and salt stress: Regulation mechanisms from whole plant to cell. *Ann. Bot.* <https://doi.org/10.1093/aob/mcn125>.
- Chen, P., Haboudane, D., Tremblay, N., Wang, J., Vigneault, P., Li, B., 2010. New spectral indicator assessing the efficiency of crop nitrogen treatment in corn and wheat. *Remote Sens Environ.* 114. <https://doi.org/10.1016/j.rse.2010.04.006>.
- Chen, Y., Lu, D., Luo, L., Pokhrel, Y., Deb, K., Huang, J., Ran, Y., 2018. Detecting irrigation extent, frequency, and timing in a heterogeneous arid agricultural region using MODIS time series, Landsat imagery, and ancillary data. *Remote Sens Environ.* 204. <https://doi.org/10.1016/j.rse.2017.10.030>.
- Chevion, B., Vervoort, R.W., Albasha, R., Dairon, R., le Priol, C., Mailhol, J.C., 2016. A framework to use crop models for multi-objective constrained optimization of irrigation strategies. *Environ. Model. Softw.* 86. <https://doi.org/10.1016/j.envsoft.2016.09.001>.
- Chevion, B., Delmas, M., Serra-Wittling, C., Dominguez-Bohorquez, J.-D., Molle, B., Lo, M., Elamri, Y., 2020. Irrigation efficiency and optimization: the Optirrig model. *Revue Science Eaux & Territoires, Water Savings in Irrigation*, 34*, 66-71.
- Chrysafis, I., Korakis, G., Kyriazopoulos, A.P., Mallinis, G., 2020. Retrieval of leaf area index using sentinel-2 imagery in a mixed mediterranean forest area. *ISPRS Int J. Geoinf.* 9. <https://doi.org/10.3390/ijgi9110622>.
- Claverie, M., Demarez, V., Duchemin, B., Hagolle, O., Ducrot, D., Marais-Sicre, C., Dejoux, J.F., Huc, M., Keravec, P., Béziat, P., Fieuzal, R., Ceschia, E., Dedieu, G., 2012. Maize and sunflower biomass estimation in southwest France using high spatial and temporal resolution remote sensing data. *Remote Sens Environ.* 124. <https://doi.org/10.1016/j.rse.2012.04.005>.
- Clevers, J.G.P.W., Vonder, O.W., Jongschaap, R.E.E., Desprats, J.F., King, C., Prvot, L., Bruguier, N., 2002. Using SPOT data for calibrating a wheat growth model under Mediterranean conditions. *Agronomie* 22. <https://doi.org/10.1051/agro:2002038>.
- Clevers, J.G.P.W., Kooistra, L., van den Brande, M.M.M., 2017. Using Sentinel-2 data for retrieving LAI and leaf and canopy chlorophyll content of a potato crop. *Remote Sens (Basel)* 9. <https://doi.org/10.3390/rs9050405>.
- Courault, D., Hadria, R., Ruget, F., Olioso, A., Duchemin, B., Hagolle, O., Dedieu, G., 2010. Combined use of FORMOSAT-2 images with a crop model for biomass and water monitoring of permanent grassland in Mediterranean region. *Hydrol. Earth Syst. Sci.* 14. <https://doi.org/10.5194/hess-14-1731-2010>.
- Courault, D., Hossard, L., Demarez, V., Dechatre, H., Irfan, K., Baghdadi, N., Flamain, F., Ruget, F., 2021. STICS crop model and Sentinel-2 images for monitoring rice growth and yield in the Camargue region. *Agron. Sustain Dev.* 41. <https://doi.org/10.1007/s13593-021-00697-w>.
- Curnel, Y., de Wit, A.J.W., Duveiller, G., Defourny, P., 2011. Potential performances of remotely sensed LAI assimilation in WOFOST model based on an OSS Experiment. *Agric. Meteorol.* 151. <https://doi.org/10.1016/j.agrformet.2011.08.002>.
- Dai, Z.Y., Li, Y.P., 2013. A multistage irrigation water allocation model for agricultural land-use planning under uncertainty. *Agric. Water Manag.* 129. <https://doi.org/10.1016/j.agwat.2013.07.013>.
- Dari, J., Brocca, L., Quintana-Seguí, P., Escorihuela, M.J., Stefan, V., Morbidelli, R., 2020. Exploiting high-resolution remote sensing soil moisture to estimate irrigation water amounts over a Mediterranean region. *Remote Sens (Basel)* 12. <https://doi.org/10.3390/rs12162593>.
- Deines, J.M., Kendall, A.D., Hyndman, D.W., 2017. Annual Irrigation Dynamics in the U. S. Northern High Plains Derived from Landsat Satellite Data. *Geophys Res Lett.* 44. <https://doi.org/10.1002/2017GL074071>.
- DeLancey, E.R., Kariyeva, J., Bried, J.T., Hird, J.N., 2019. Large-scale probabilistic identification of boreal peatlands using Google Earth Engine, open-access satellite data, and machine learning. *PLoS One* 14. <https://doi.org/10.1371/journal.pone.0218165>.
- Demarez, V., Helen, F., Marais-Sicre, C., Baup, F., 2019. In-season mapping of irrigated crops using Landsat 8 and Sentinel-1 time series. *Remote Sens (Basel)* 11. <https://doi.org/10.3390/rs11020118>.
- Dente, L., Satalino, G., Mattia, F., Rinaldi, M., 2008. Assimilation of leaf area index derived from ASAR and MERIS data into CERES-Wheat model to map wheat yield. *Remote Sens Environ.* 112. <https://doi.org/10.1016/j.rse.2007.05.023>.
- Dheeravath, V., Thenkabail, P.S., Chandranthana, G., Noojipady, P., Reddy, G.P.O., Biradar, C.M., Gumma, M.K., Velpuri, M., 2010. Irrigated areas of India derived using MODIS 500 m time series for the years 2001-2003. *ISPRS J. Photogramm. Remote Sens.* 65. <https://doi.org/10.1016/j.isprsjprs.2009.08.004>.
- Duchemin, B., Boulet, G., Maisongrande, P., Benhadj, I., Hadria, R., Khabba, S., Chehbouni, A., Ezzahar, J., Olioso, A., 2005. Un modèle simplifié pour l'estimation du rendement de cultures céréalières en milieu semi-aride. In: *Un Modèle Simplifié*

- Pour l'estimation Du Bilan Hydrique et Du Rendement de Cultures Céréalières En Milieu Semi-Aride.
- Duchemin, B., Hadria, R., Erraki, S., Boulet, G., Maisongrande, P., Chehbouni, A., Escadafal, R., Ezzahar, J., Hoedjes, J.C.B., Kharrou, M.H., Khabba, S., Mougenot, B., Olioso, A., Rodriguez, J.C., Simonneaux, V., 2006. Monitoring wheat phenology and irrigation in Central Morocco: On the use of relationships between evapotranspiration, crops coefficients, leaf area index and remotely-sensed vegetation indices. *Agric. Water Manag* 79. <https://doi.org/10.1016/j.agwat.2005.02.013>.
- Duchemin, B., Maisongrande, P., Boulet, G., Benhadj, I., 2008. A simple algorithm for yield estimates: Evaluation for semi-arid irrigated winter wheat monitored with green leaf area index. *Environ. Model. Softw.* 23. <https://doi.org/10.1016/j.envsoft.2007.10.003>.
- Duchemin, B., Fieuzal, R., Rivera, M.A., Ezzahar, J., Jarlan, L., Rodriguez, J.C., Hagolle, O., Watts, C., 2015. Impact of sowing date on yield and water use efficiency of wheat analyzed through spatial modeling and FORMOSAT-2 images. *Remote Sens (Basel)* 7. <https://doi.org/10.3390/rs70505951>.
- Efeoglu, B., Ekmekci, Y., Cicek, N., 2009. Physiological responses of three maize cultivars to drought stress and recovery. *South Afr. J. Bot.* 75. <https://doi.org/10.1016/j.sajb.2008.06.005>.
- El Hajj, M., Baghdadi, N., Belaud, G., Zribi, M., Cheviron, B., Courault, D., Hagolle, O., Charron, F., 2014. Irrigated grassland monitoring using a time series of TerraSAR-X and COSMO-SkyMed X-Band SAR data. *Remote Sens (Basel)* 6. <https://doi.org/10.3390/rs61010002>.
- El Hajj, M., Baghdadi, N., Zribi, M., Belaud, G., Cheviron, B., Courault, D., Charron, F., 2016. Soil moisture retrieval over irrigated grassland using X-band SAR data. *Remote Sens Environ.* 176. <https://doi.org/10.1016/j.rse.2016.01.027>.
- El Hajj, M., el Baghdadi, N., Zribi, M., Bazzi, H., 2017. Synergic use of Sentinel-1 and Sentinel-2 images for operational soil moisture mapping at high spatial resolution over agricultural areas. *Remote Sens (Basel)* 9. <https://doi.org/10.3390/rs9121292>.
- El Hajj, M., Baghdadi, N., Bazzi, H., Zribi, M., 2019. Penetration analysis of SAR signals in the C and L bands for wheat, maize, and grasslands. *Remote Sens (Basel)* 11. <https://doi.org/10.3390/rs11010031>.
- Elliott, J., Deryng, D., Müller, C., Frieler, K., Konzmann, M., Gerten, D., Glotter, M., Flörke, M., Wada, Y., Best, N., Eisner, S., Fekete, B.M., Folberth, C., Foster, I., Gosling, S.N., Haddeland, I., Khabarov, N., Ludwig, F., Masaki, Y., Olin, S., Rosenzweig, C., Ruane, A.C., Satoh, Y., Schmid, E., Stacke, T., Tang, Q., Wisser, D., 2014. Constraints and potentials of future irrigation water availability on agricultural production under climate change. *Proc. Natl. Acad. Sci. USA* 111. <https://doi.org/10.1073/pnas.1222474110>.
- Ercin, E., Chico, D., Chapagain, A.K., 2019. Vulnerabilities of the European Union's economy to hydrological extremes outside its borders. *Atmosphere (Basel)* 10. <https://doi.org/10.3390/atmos10100593>.
- Farooq, M., Bramley, H., Palta, J.A., Siddique, K.H.M., 2011. Heat stress in wheat during reproductive and grain-filling phases. *CRC Crit. Rev. Plant Sci.* <https://doi.org/10.1080/07352689.2011.615687>.
- Feng, R., Zhang, Y., Yu, W., Hu, W., Wu, J., Ji, R., Wang, H., Zhao, X., 2013. Analysis of the relationship between the spectral characteristics of maize canopy and leaf area index under drought stress. *Acta Ecol. Sin.* 33. <https://doi.org/10.1016/j.chnaes.2013.09.001>.
- Fieuzal, R., Duchemin, B., Jarlan, L., Zribi, M., Baup, F., Merlin, O., Hagolle, O., Garatuzza-Payan, J., 2011. Combined use of optical and radar satellite data for the monitoring of irrigation and soil moisture of wheat crops. *Hydrol. Earth Syst. Sci.* 15. <https://doi.org/10.5194/hess-15-1117-2011>.
- Fischer, R.A., Byerlee, D., Edmeades, G.O., 2014. Crop yields and global food security: will yield increase continue to feed the world? Australian Centre for International Agricultural Research. Canberra. Research, Canberra.
- Fisher, J.L., Mustard, J.F., Vadeboncoeur, M.A., 2006. Green leaf phenology at Landsat resolution: Scaling from the field to the satellite. *Remote Sens Environ.* 100. <https://doi.org/10.1016/j.rse.2005.10.022>.
- Gao, Q., Zribi, M., Escorihuela, M.J., Baghdadi, N., Segui, P.Q., 2018. Irrigation mapping using Sentinel-1 time series at field scale. *Remote Sens (Basel)* 10. <https://doi.org/10.3390/rs10091495>.
- García y García, Guerra, A., Hoogenboom, L.C., G., 2009. Water use and water use efficiency of sweet corn under different weather conditions and soil moisture regimes. *Agric. Water Manag.* <https://doi.org/10.1016/j.agwat.2009.04.022>.
- Garrison, M. v. Batchelor, W.D., Kanwar, R.S., Ritchie, J.T., 1999. Evaluation of the CERES-Maize water and nitrogen balances under tile-drained conditions. *Agric. Syst.* 62. [https://doi.org/10.1016/S0308-521X\(99\)00064-5](https://doi.org/10.1016/S0308-521X(99)00064-5).
- Ge, Y., Li, X., Huang, C., Nan, Z., 2013. A Decision Support System for irrigation water allocation along the middle reaches of the Heihe River Basin, Northwest China. *Environ. Model. Softw.* 47. <https://doi.org/10.1016/j.envsoft.2013.05.010>.
- Godfray, H.C.J., Beddington, J.R., Crute, I.R., Haddad, L., Lawrence, D., Muir, J.F., Pretty, J., Robinson, S., Thomas, S.M., Toulmin, C., 2010. Food security: The challenge of feeding 9 billion people. *Science (1979)*. <https://doi.org/10.1126/science.1185383>.
- Guérif, M., Duke, C.L., 2000. Adjustment procedures of a crop model to the site specific characteristics of soil and crop using remote sensing data assimilation. *Agric. Ecosyst. Environ.* 81. [https://doi.org/10.1016/S0167-8809\(00\)00168-7](https://doi.org/10.1016/S0167-8809(00)00168-7).
- Guerra, L.C., García y García, Hook, A., Harrison, J.E., Thomas, K.A., Stooksbury, D.L., Hoogenboom, D.E., G., 2007. Irrigation water use estimates based on crop simulation models and kriging. *Agric. Water Manag* 89. <https://doi.org/10.1016/j.agwat.2007.01.010>.
- Gumma, M.K., Thenkabail, P.S., Hideto, F., Nelson, A., Dheeravath, V., Busia, D., Rala, A., 2011. Mapping irrigated areas of Ghana using fusion of 30 m and 250 m resolution remote-sensing data. *Remote Sens (Basel)* 3. <https://doi.org/10.3390/rs3040816>.
- Hadria, R., Duchemin, B., Lahrouni, A., Khabba, S., Er-Raki, S., Dedieu, G., Chehbouni, A. G., Olioso, A., 2006. Monitoring of irrigated wheat in a semi-arid climate using crop modelling and remote sensing data: Impact of satellite revisit time frequency. *Int. J. Remote Sens* 27. <https://doi.org/10.1080/01431160500382980>.
- Hagolle, O., Morin, D., Kadiri, M., 2018. Detailed Processing Model for the Weighted Average Synthesis Processor (WASP) (Version 1.4). Zenodo. <https://doi.org/10.5281/zenodo.1401360>.
- Hamze, M., Baghdadi, N., el Hajj, M.M., Zribi, M., Bazzi, H., Cheviron, B., Faour, G., 2021. Integration of l-band derived soil roughness into a bare soil moisture retrieval approach from c-band sar data. *Remote Sens (Basel)* 13. <https://doi.org/10.3390/rs13121202>.
- Han, D., Wang, P., Tansey, K., Zhang, S., Tian, H., Zhang, Y., Li, H., 2021. Improving Wheat Yield Estimates by Integrating a Remotely Sensed Drought Monitoring Index into the Simple Algorithm for Yield Estimate Model. *IEEE J. Sel. Top. Appl. Earth Obs. Remote Sens* 14. <https://doi.org/10.1109/JSTARS.2021.3119398>.
- Holzworth, D.P., Huth, N.I., deVoil, P.G., Zurcher, E.J., Herrmann, N.I., McLean, G., Chenu, K., van Oosterom, E.J., Snow, V., Murphy, C., Moore, A.D., Brown, H., Whish, J.P.M., Verrall, S., Fainges, J., Bell, L.W., Peake, A.S., Poulton, P.L., Hochman, Z., Thorburn, P.J., Gaydon, D.S., Dalgliesh, N.P., Rodriguez, D., Cox, H., Chapman, S., Doherty, A., Teixeira, E., Sharp, J., Cichota, R., Vogel, I., Li, F.Y., Wang, E., Hammer, G.L., Robertson, M.J., Dimes, J.P., Whitbread, A.M., Hunt, J., van Rees, H., McClelland, T., Carberry, P.S., Hargreaves, J.N.G., MacLeod, N., McDonald, C., Harsdorf, J., Wedgwood, S., Keating, B.A., 2014. APSIM - Evolution towards a new generation of agricultural systems simulation. *Environ. Model. Softw.* 62. <https://doi.org/10.1016/j.envsoft.2014.07.009>.
- Hoogenboom, G., 2000. Contribution of agrometeorology to the simulation of crop production and its applications. *Agric. For. Meteorol.* [https://doi.org/10.1016/S0168-1923\(00\)00108-8](https://doi.org/10.1016/S0168-1923(00)00108-8).
- Hoogenboom, G., Porter, C.H., Boote, K.J., Shelia, V., Wilkens, P.W., Singh, U., White, J. W., Asseng, S., Lizaso, J.I., Moreno, L.P., Pavan, W., Ogoshi, R., Hunt, L.A., Tsuji, G. Y., Jones, J.W., 2019. DSSAT Crop Model. *Ecosyst.* <https://doi.org/10.19103/as.2019.0061.10>.
- Hook, J.E., 1994. Using crop models to plan water withdrawals for irrigation in drought years. *Agric. Syst.* 45. [https://doi.org/10.1016/0308-521X\(94\)90142-3](https://doi.org/10.1016/0308-521X(94)90142-3).
- Hsiao, T.C., Heng, L., Steduto, P., Rojas-Lara, B., Raes, D., Fereres, E., 2009. Aquacrop-The FAO crop model to simulate yield response to water: III. Parameterization and testing for maize. *Agron. J.* 101. <https://doi.org/10.2134/agronj2008.0218s>.
- Huang, C., Ma, S., Gao, Y., Liu, Z., Zhai, Q., Zhao, B., Ning, D., Duan, A., Liu, X., Chen, H., Liu, Z., 2022. Response of Summer Maize Growth and Water Use to Different Irrigation Regimes. *Agronomy* 12. <https://doi.org/10.3390/agronomy12040768>.
- Huang, J., Tang, S., Ousama, A.I., Wang, R., 2001. Integration of remote sensing data and simulation model to estimate rice yield: in: 2001 International Conferences on Info-Tech and Info-Net: A Key to Better Life, ICII 2001 - Proceedings. <https://doi.org/10.1109/ICII.2001.982729>.
- Huang, J., Ma, H., Su, W., Zhang, X., Huang, Y., Fan, J., Wu, W., 2015. Jointly Assimilating MODIS LAI and et Products into the SWAP Model for Winter Wheat Yield Estimation. *IEEE J. Sel. Top. Appl. Earth Obs. Remote Sens* 8. <https://doi.org/10.1109/JSTARS.2015.2403135>.
- Huang, J., Sedano, F., Huang, Y., Ma, H., Li, X., Liang, S., Tian, L., Zhang, X., Fan, J., Wu, W., 2016. Assimilating a synthetic Kalman filter leaf area index series into the WOFOST model to improve regional winter wheat yield estimation. *Agric. Meteorol.* 216. <https://doi.org/10.1016/j.agrformet.2015.10.013>.
- Huang, J., Gómez-Dans, J.L., Huang, H., Ma, H., Wu, Q., Lewis, P.E., Liang, S., Chen, Z., Xue, J.H., Wu, Y., Zhao, F., Wang, J., Xie, X., 2019. Assimilation of remote sensing into crop growth models: Current status and perspectives. *Agric. Meteorol.* <https://doi.org/10.1016/j.agrformet.2019.06.008>.
- Hubert, B., Rosegrant, M., van Boekel, M.A.J.S., Ortiz, R., 2010. The future of food: Scenarios for 2050. *Crop Sci.* 50. <https://doi.org/10.2135/cropsci2009.09.0530>.
- Ines, A.V.M., Das, N.N., Hansen, J.W., Njoku, E.G., 2013. Assimilation of remotely sensed soil moisture and vegetation with a crop simulation model for maize yield prediction. *Remote Sens Environ.* 138. <https://doi.org/10.1016/j.rse.2013.07.018>.
- Jin, X., Kumar, L., Li, Z., Feng, H., Xu, X., Yang, G., Wang, J., 2018. A review of data assimilation of remote sensing and crop models. *Eur. J. Agron.* <https://doi.org/10.1016/j.eja.2017.11.002>.
- Jin, X., Li, Z., Feng, H., Ren, Z., Li, S., 2020. Deep neural network algorithm for estimating maize biomass based on simulated Sentinel 2A vegetation indices and leaf area index. *Crop J.* 8. <https://doi.org/10.1016/j.cj.2019.06.005>.
- Jones, J.W., Tsuji, G.Y., Hoogenboom, G., Hunt, L.A., Thornton, P.K., Wilkens, P.W., Imamura, D.T., Bowen, W.T., Singh, U., 1998. Decis. Support Syst. *agrotechnology Transf.: DSSAT v3.* https://doi.org/10.1007/978-94-017-3624-4_8.
- Jones, J.W., Hoogenboom, G., Porter, C.H., Boote, K.J., Batchelor, W.D., Hunt, L.A., Wilkens, P.W., Singh, U., Gijssman, A.J., Ritchie, J.T., 2003. The DSSAT cropping system model. *Eur. J. Agron.* [https://doi.org/10.1016/S1161-0301\(02\)00107-7](https://doi.org/10.1016/S1161-0301(02)00107-7).
- Jongschaap, R.E.E., Schouten, L.S.M., 2005. Predicting wheat production at regional scale by integration of remote sensing data with a simulation model. *Agron. Sustain. Dev.* 25. <https://doi.org/10.1051/agro:2005048>.
- Kang, Y., Özdoğan, M., 2019. Field-level crop yield mapping with Landsat using a hierarchical data assimilation approach. *Remote Sens Environ.* 228. <https://doi.org/10.1016/j.rse.2019.04.005>.
- Kettler, T.A., Doran, J.W., Gilbert, T.L., 2001. Simplified Method for Soil Particle-Size Determination to Accompany Soil-Quality Analyses. *Soil Sci. Soc. Am. J.* 65. <https://doi.org/10.2136/sssaj2001.653849x>.

- Köksal, E.S., 2011. Hyperspectral reflectance data processing through cluster and principal component analysis for estimating irrigation and yield related indicators. *Agric. Water Manag* 98. <https://doi.org/10.1016/j.agwat.2011.03.014>.
- le Page, M., Toumi, J., Khabba, S., Hagolle, O., Tavernier, A., Hakim Kharrou, M., Er-Raki, S., Huc, M., Kasbani, M., Moutamanni, A., el, Yousfi, M., Jarlan, L., 2014. A life-size and near real-time test of irrigation scheduling with a sentinel-2 like time series (SPOT4-Take5) in Morocco. *Remote Sens (Basel)* 6. <https://doi.org/10.3390/rs6111182>.
- le Page, M., Jarlan, L., el Hajj, M.M., Zribi, M., Baghdadi, N., Boone, A., 2020. Potential for the detection of irrigation events on maize plots using Sentinel-1 soil moisture products. *Remote Sens (Basel)* 12. <https://doi.org/10.3390/rs12101621>.
- Leys, C., Ley, C., Klein, O., Bernard, P., Licata, L., 2013. Detecting outliers: Do not use standard deviation around the mean, use absolute deviation around the median. *J. Exp. Soc. Psychol.* 49. <https://doi.org/10.1016/j.jesp.2013.03.013>.
- Li, T., Hasegawa, T., Yin, X., Zhu, Y., Boote, K., Adam, M., Bregaglio, S., Buis, S., Confalonieri, R., Fumoto, T., Gaydon, D., Marcaida, M., Nakagawa, H., Oriol, P., Ruane, A.C., Ruget, F., Singh, B., Singh, U., Tang, L., Tao, F., Wilkens, P., Yoshida, H., Zhang, Z., Bouman, B., 2015. Uncertainties in predicting rice yield by current crop models under a wide range of climatic conditions. *Glob. Chang Biol.* 21. <https://doi.org/10.1111/gcb.12758>.
- Liebisch, F., Kirchgessner, N., Schneider, D., Walter, A., Hund, A., 2015. Remote, aerial phenotyping of maize traits with a mobile multi-sensor approach. *Plant Methods* 11. <https://doi.org/10.1186/s13007-015-0048-8>.
- Lobell, D.B., Bänziger, M., Magorokosho, C., Vivek, B., 2011. Nonlinear heat effects on African maize as evidenced by historical yield trials. *Nat. Clim. Chang* 1. <https://doi.org/10.1038/nclimate1043>.
- López-Cedrón, F.X., Boote, K.J., Piñeiro, J., Sau, F., 2008. Improving the CERES-maize model ability to simulate water deficit impact on maize production and yield components. *Agron. J.* 100. <https://doi.org/10.2134/agronj2007.0088>.
- Maas, S.J., 1988. Use of remotely-sensed information in agricultural crop growth models. *Ecol. Model.* 41. [https://doi.org/10.1016/0304-3800\(88\)90031-2](https://doi.org/10.1016/0304-3800(88)90031-2).
- Mailhol, J.C., Olufayo, A.A., Ruelle, P., 1997. Sorghum and sunflower evapotranspiration and yield from simulated leaf area index. *Agric. Water Manag* 35. [https://doi.org/10.1016/S0378-3774\(97\)00029-2](https://doi.org/10.1016/S0378-3774(97)00029-2).
- Mailhol, J.C., Ruelle, P., Walsler, S., Schütze, N., Dejean, C., 2011. Analysis of AET and yield predictions under surface and buried drip irrigation systems using the Crop Model PILOTE and Hydrus-2D. *Agric. Water Manag* 98. <https://doi.org/10.1016/j.agwat.2011.01.014>.
- Mailhol, J.C., Albasha, R., Cheviron, B., Lopez, J.M., Ruelle, P., Dejean, C., 2018. The PILOTE-N model for improving water and nitrogen management practices: Application in a Mediterranean context. *Agric. Water Manag* 204. <https://doi.org/10.1016/j.agwat.2018.04.015>.
- Mekonnen, M.M., Hoekstra, A.Y., 2014. Water footprint benchmarks for crop production: A first global assessment. *Ecol. Indic.* 46. <https://doi.org/10.1016/j.ecolind.2014.06.013>.
- Mekonnen, M.M., Hoekstra, A.Y., 2016. Sustainability: Four billion people facing severe water scarcity. *Sci. Adv.* 2. <https://doi.org/10.1126/sciadv.1500323>.
- Monaco, E., Bonfante, A., Alfieri, S.M., Basile, A., Menenti, M., de Lorenzi, F., 2014. Climate change, effective water use for irrigation and adaptability of maize: A case study in southern Italy. *Biosyst. Eng.* 128. <https://doi.org/10.1016/j.biosystemseng.2014.09.001>.
- Mullen, J.D., Yu, Y., Hoogenboom, G., 2009. Estimating the demand for irrigation water in a humid climate: A case study from the southeastern United States. *Agric. Water Manag* 96. <https://doi.org/10.1016/j.agwat.2009.04.003>.
- Myers, S.S., Smith, M.R., Guth, S., Golden, C.D., Vaitla, B., Mueller, N.D., Dangour, A.D., Huybers, P., 2017. Climate Change and Global Food Systems: Potential Impacts on Food Security and Undernutrition. *Annu Rev. Public Health.* <https://doi.org/10.1146/annurev-pubhealth-031816-044356>.
- Nathan, A.J., Scobell, A., 2012. How China sees America. *Foreign Affairs.*
- Ndikumana, E., Minh, D.H.T., Baghdadi, N., Courault, D., Hossard, L., 2018. Deep recurrent neural network for agricultural classification using multitemporal SAR Sentinel-1 for Camargue, France. *Remote Sens (Basel)* 10. <https://doi.org/10.3390/rs10081217>.
- Nijbroek, R., Hoogenboom, G., Jones, J.W., 2003. Optimizing irrigation management for a spatially variable soybean field. *Agric. Syst.* 76. [https://doi.org/10.1016/S0308-521X\(02\)00127-0](https://doi.org/10.1016/S0308-521X(02)00127-0).
- Ouaadi, N., Jarlan, L., Khabba, S., Ezzahar, J., le Page, M., Merlin, O., 2021. Irrigation amounts and timing retrieval through data assimilation of surface soil moisture into the fao-56 approach in the south mediterranean region. *Remote Sens (Basel)* 13. <https://doi.org/10.3390/rs13142667>.
- Ozdogan, M., 2011. Exploring the potential contribution of irrigation to global agricultural primary productivity. *Glob. Biogeochem. Cycles* 25. <https://doi.org/10.1029/2009GB003720>.
- Ozdogan, M., Gutman, G., 2008. A new methodology to map irrigated areas using multi-temporal MODIS and ancillary data: An application example in the continental US. *Remote Sens Environ.* 112. <https://doi.org/10.1016/j.rse.2008.04.010>.
- Ozdogan, M., Yang, Y., Allez, G., Cervantes, C., 2010. Remote sensing of irrigated agriculture: Opportunities and challenges. *Remote Sens (Basel).* <https://doi.org/10.3390/rs2092274>.
- Pageot, Y., Baup, F., Inglada, J., Baghdadi, N., Demarez, V., 2020. Detection of irrigated and rainfed crops in temperate areas using sentinel-1 and sentinel-2 time series. *Remote Sens (Basel)* 12. <https://doi.org/10.3390/rs12183044>.
- Palosuo, T., Kersebaum, K.C., Angulo, C., Hlavinka, P., Moriondo, M., Olesen, J.E., Patil, R.H., Ruget, F., Rumbaer, C., Takáč, J., Trnka, M., Bindi, M., Čalada, B., Ewert, F., Ferrise, R., Mirschel, W., Şaylan, L., Šiška, B., Rötter, R., 2011. Simulation of winter wheat yield and its variability in different climates of Europe: A comparison of eight crop growth models. *Eur. J. Agron.* 35. <https://doi.org/10.1016/j.eja.2011.05.001>.
- Pervez, M.S., Brown, J.F., 2010. Mapping irrigated lands at 250-m scale by merging MODIS data and National Agricultural Statistics. *Remote Sens (Basel)* 2. <https://doi.org/10.3390/rs2102388>.
- Piscitelli, L., Colovic, M., Aly, A., Hamze, M., Todorovic, M., Cantore, V., Albrizio, R., 2022. Correction to: Piscitelli et al. Adaptive Agricultural Strategies for Facing Water Deficit in Sweet Maize Production: A Case Study of a Semi-Arid Mediterranean Region. *Water* 2021, 13, 3285. *Water (Switzerland)*. <https://doi.org/10.3390/w14050679>.
- Pôças, I., Paço, T.A., Paredes, P., Cunha, M., Pereira, L.S., 2015. Estimation of actual crop coefficients using remotely sensed vegetation indices and soil water balance modelled data. *Remote Sens (Basel)* 7. <https://doi.org/10.3390/rs70302373>.
- Pokhrel, Y.N., Hanasaki, N., Wada, Y., Kim, H., 2016. Recent progresses in incorporating human land–water management into global land surface models toward their integration into Earth system models. *Wiley Interdiscip. Rev.: Water.* <https://doi.org/10.1002/wat2.1150>.
- Rötter, R.P., Palosuo, T., Kersebaum, K.C., Angulo, C., Bindi, M., Ewert, F., Ferrise, R., Hlavinka, P., Moriondo, M., Nendel, C., Olesen, J.E., Patil, R.H., Ruget, F., Takáč, J., Trnka, M., 2012. Simulation of spring barley yield in different climatic zones of Northern and Central Europe: A comparison of nine crop models. *Field Crops Res* 133. <https://doi.org/10.1016/j.fcr.2012.03.016>.
- Saadi, S., Simonneaux, V., Boulet, G., Raimbault, B., Mougnot, B., Fanise, P., Ayari, H., Lili-Chabaane, Z., 2015. Monitoring irrigation consumption using high resolution NDVI image time series: Calibration and validation in the Kairouan plain (Tunisia). *Remote Sens (Basel)* 7. <https://doi.org/10.3390/rs71013005>.
- Salmon, J.M., Friedl, M.A., Frolking, S., Wisser, D., Douglas, E.M., 2015. Global rain-fed, irrigated, and paddy croplands: A new high resolution map derived from remote sensing, crop inventories and climate data. *Int. J. Appl. Earth Obs. Geoinf.* 38. <https://doi.org/10.1016/j.jag.2015.01.014>.
- Schlüter, U., Mascher, M., Colmsee, C., Scholz, U., Bräutigam, A., Fahnenstich, H., Sonnewald, U., 2012. Maize source leaf adaptation to nitrogen deficiency affects not only nitrogen and carbon metabolism but also control of phosphate homeostasis. *Plant Physiol.* 160. <https://doi.org/10.1104/pp.112.204420>.
- Schneider, K., 2003. Assimilating remote sensing data into a land-surface process model. *Int. J. Remote Sens* 24. <https://doi.org/10.1080/01431160210154803>.
- Sellami, M.H., Albrizio, R., Colović, M., Hamze, M., Cantore, V., Todorovic, M., Piscitelli, L., Stellacci, A.M., 2022. Selection of Hyperspectral Vegetation Indices for Monitoring Yield and Physiological Response in Sweet Maize under Different Water and Nitrogen Availability. *Agronomy* 12. <https://doi.org/10.3390/agronomy12020489>.
- Si, Z., Zain, M., Mehmood, F., Wang, G., Gao, Y., Duan, A., 2020. Effects of nitrogen application rate and irrigation regime on growth, yield, and water-nitrogen use efficiency of drip-irrigated winter wheat in the North China Plain. *Agric. Water Manag* 231. <https://doi.org/10.1016/j.agwat.2020.106002>.
- Silvestro, P.C., Pignatti, S., Yang, H., Yang, G., Pascucci, S., Castaldi, F., Casa, R., 2017. Sensitivity analysis of the Aquacrop and SAFYE crop models for the assessment of water limited winter wheat yield in regional scale applications. *PLoS One* 12. <https://doi.org/10.1371/journal.pone.0187485>.
- Skuras, D., Psaltopoulos, D., 2012. A broad overview of the main problems derived from climate change that will affect agricultural production in the Mediterranean area. *Building resilience for adaptation to climate change in the agriculture sector. Proc. a Jt. FAO/OECD Workshop.*
- Soil Survey Manual, 2017, Soil Survey Manual (SSM) | NRCS Soils. Usda.
- Steduto, P., Hsiao, T.C., Raes, D., Fereres, E., 2009. Aquacrop—the FAO crop model to simulate yield response to water: I. concepts and underlying principles. *Agron. J.* 101, 426–437. <https://doi.org/10.2134/agronj2008.0139s>.
- Stöckle, C.O., Donatelli, M., Nelson, R., 2003. CropSyst, a cropping systems simulation model. *Eur. J. Agron.* [https://doi.org/10.1016/S1161-0301\(02\)00109-0](https://doi.org/10.1016/S1161-0301(02)00109-0).
- Tewes, A., Montzka, C., Nolte, M., Krauss, G., Hoffmann, H., Gaiser, T., 2020. Assimilation of sentinel-2 estimated lai into a crop model: Influence of timing and frequency of acquisitions on simulation of water stress and biomass production of winter wheat. *Agronomy* 10. <https://doi.org/10.3390/agronomy10111813>.
- Thenkabail, P.S., Schull, M., Turrall, H., 2005. Ganges and Indus river basin land use/land cover (LULC) and irrigated area mapping using continuous streams of MODIS data. *Remote Sens Environ.* 95. <https://doi.org/10.1016/j.rse.2004.12.018>.
- Thorp, K.R., Hunsaker, D.J., French, A.N., 2010. Assimilating leaf area index estimates from remote sensing into the simulations of a cropping systems model. *Trans. ASABE* 53.
- Tilman, D., Clark, M., 2015. Food, agriculture & the environment: Can we feed the world & save the earth? *Daedalus* 144. https://doi.org/10.1162/DAED_a_00350.
- Tilman, D., Balzer, C., Hill, J., Befort, B.L., 2011. Global food demand and the sustainable intensification of agriculture. *Proc. Natl. Acad. Sci. USA* 108. <https://doi.org/10.1073/pnas.1116437108>.
- Toureiro, C., Serralheiro, R., Shahidian, S., Sousa, A., 2017. Irrigation management with remote sensing: Evaluating irrigation requirement for maize under Mediterranean climate condition. *Agric. Water Manag* 184. <https://doi.org/10.1016/j.agwat.2016.02.010>.
- Tripathy, R., Chaudhari, K.N., Mukherjee, J., Ray, S.S., Patel, N.K., Panigrahy, S., Singh Parihar, J., 2013. Forecasting wheat yield in Punjab state of India by combining crop simulation model WOFOST and remotely sensed inputs. *Remote Sens. Lett.* 4. <https://doi.org/10.1080/2150704X.2012.683117>.
- Varella, H., Buis, S., Launay, M., Guérif, M., 2012. Global sensitivity analysis for choosing the main soil parameters of a crop model to be determined. *Agric. Sci.* 03. <https://doi.org/10.4236/as.2012.37116>.

- Velpuri, N.M., Thenkabail, P.S., Gumma, M.K., Biradar, C., Dheeravath, V., Noojipady, P., Yuanjie, L., 2009. Influence of resolution in irrigated area mapping and area estimation. *Photo Eng. Remote Sens.* 75. <https://doi.org/10.14358/PERS.75.12.1383>.
- Wallach, D., Martre, P., Liu, B., Asseng, S., Ewert, F., Thorburn, P.J., van Ittersum, M., Aggarwal, P.K., Ahmed, M., Basso, B., Biernath, C., Cammarano, D., Challinor, A.J., de Sanctis, G., Dumont, B., Eyshi Rezaei, E., Fereres, E., Fitzgerald, G.J., Gao, Y., Garcia-Vila, M., Gayler, S., Girousse, C., Hoogenboom, G., Horan, H., Izaurralde, R. C., Jones, C.D., Kassie, B.T., Kersebaum, K.C., Klein, C., Koehler, A.K., Maiorano, A., Minoli, S., Müller, C., Naresh Kumar, S., Nendel, C., O'Leary, G.J., Palosuo, T., Priesack, E., Ripoche, D., Rötter, R.P., Semenov, M.A., Stöckle, C., Stratonovitch, P., Streck, T., Supit, I., Tao, F., Wolf, J., Zhang, Z., 2018. Multimodel ensembles improve predictions of crop–environment–management interactions. *Glob. Chang Biol.* 24. <https://doi.org/10.1111/gcb.14411>.
- Wang, J., Li, X., Lu, L., Fang, F., 2013. Estimating near future regional corn yields by integrating multi-source observations into a crop growth model. *Eur. J. Agron.* 49. <https://doi.org/10.1016/j.eja.2013.03.005>.
- Weiss, M., Baret, F., 2016. S2ToolBox Level 2 products: LAI, FAPAR, FCOVER - Version 1.1. Sentinel2 ToolBox Level2 Products.
- Weiss, M., Baret, F., Smith, G.J., Jonckheere, I., Coppin, P., 2004. Review of methods for in situ leaf area index (LAI) determination Part II. Estimation of LAI, errors and sampling. *Agric. Meteorol.* 121. <https://doi.org/10.1016/j.agrformet.2003.08.001>.
- de Wit, A., Boogaard, H., Fumagalli, D., Janssen, S., Knapen, R., van Kraalingen, D., Supit, I., van der Wijngaart, R., van Diepen, K., 2019. 25 years of the WOFOST cropping systems model. *Agric. Syst.* <https://doi.org/10.1016/j.agry.2018.06.018>.
- Wu, X., Zhou, J., Wang, H., Li, Y., Zhong, B., 2015. Evaluation of irrigation water use efficiency using remote sensing in the middle reach of the Heihe river, in the semi-arid Northwestern China. *Hydrol. Process.* 29. <https://doi.org/10.1002/hyp.10365>.
- Xiang, K., Ma, M., Liu, W., Dong, J., Zhu, X., Yuan, W., 2019. Mapping irrigated areas of northeast China in comparison to natural vegetation. *Remote Sens (Basel)* 11. <https://doi.org/10.3390/rs11070825>.
- Yao, F., Tang, Y., Wang, P., Zhang, J., 2015. Estimation of maize yield by using a process-based model and remote sensing data in the Northeast China Plain. *Phys. Chem. Earth* 87–88. <https://doi.org/10.1016/j.pce.2015.08.010>.
- Zhang, C., Liu, J., Dong, T., Pattey, E., Shang, J., Tang, M., Cai, H., Saddique, Q., 2019. Coupling hyperspectral remote sensing data with a crop model to study winter wheat water demand. *Remote Sens (Basel)* 11. <https://doi.org/10.3390/rs11141684>.
- Zheng, G., Moskal, L.M., 2009. Retrieving Leaf Area Index (LAI) Using Remote Sensing: Theories, Methods and Sensors. *Sensors.* <https://doi.org/10.3390/s90402719>.
- Zhou, H., Zhou, G., He, Q., Zhou, L., Ji, Y., Zhou, M., 2020. Environmental explanation of maize specific leaf area under varying water stress regimes. *Environ. Exp. Bot.* 171. <https://doi.org/10.1016/j.envexpbot.2019.103932>.
- Zhuo, W., Huang, J., Li, L., Zhang, X., Ma, H., Gao, X., Huang, H., Xu, B., Xiao, X., 2019. Assimilating Soil Moisture Retrieved from Sentinel-1 and Sentinel-2 Data into WOFOST Model to Improve Winter Wheat Yield Estimation. *Remote Sens (Basel)* 11. <https://doi.org/10.3390/rs11131618>.
- Zribi, M., Dechambre, M., 2003. A new empirical model to retrieve soil moisture and roughness from C-band radar data. *Remote Sens Environ.* 84. [https://doi.org/10.1016/S0034-4257\(02\)00069-X](https://doi.org/10.1016/S0034-4257(02)00069-X).
- Zwart, S.J., Bastiaanssen, W.G.M., de Fraiture, C., Molden, D.J., 2010. WATPRO: A remote sensing based model for mapping water productivity of wheat. *Agric. Water Manag.* 97. <https://doi.org/10.1016/j.agwat.2010.05.017>.